Biochemistry

Article

Cite This: Biochemistry 2019, 58, 546−560

pubs.acs.org/biochemistry

Use of Circular Statistics To Model αMan-(1→2)-αMan and αMan-(1→3)-α/βMan *O*-Glycosidic Linkage Conformation in ^{13}C-Labeled Disaccharides and High-Mannose Oligosaccharides

Wenhui Zhang,[†] Reagan Meredith,[†] Qingfeng Pan,[†] Xiaocong Wang,[§] Robert J. Woods,[§] Ian Carmichael,[‡] and Anthony S. Serianni*[,†]

[†]Department of Chemistry and Biochemistry, and [‡]Radiation Laboratory, University of Notre Dame, Notre Dame, Indiana 46556-5670 United States

[§]Complex Carbohydrate Research Center, University of Georgia, Athens, Georgia 30602 United States

Supporting Information

ABSTRACT: A new experimental method, *MA'AT* analysis, has been applied to investigate the conformational properties of *O*-glycosidic linkages in several biologically important mannose-containing di- and oligosaccharides. Methyl α-D-mannopyranosyl-(1→2)-α-D-mannopyranoside (**2**), methyl α-D-mannopyranosyl-(1→3)-α-D-mannopyranoside (**3**), and methyl α-D-mannopyranosyl-(1→3)-β-D-mannopyranoside (**4**) were prepared with selective ^{13}C-enrichment to enable the measurement of NMR scalar couplings across their internal *O*-glycosidic linkages. Density functional theory (DFT) was used to parameterize equations for J_{CH} and J_{CC} values in **2**−**4** that are sensitive to phi (ϕ) and psi (ψ). The experimental *J*-couplings and parameterized equations were treated using a circular statistics algorithm encoded in the *MA'AT* program. Conformations about ϕ and ψ treated using single-state von Mises models gave excellent fits to the ensembles of redundant *J*-couplings. Mean values and circular standard deviations (CSDs) for each linkage torsion angle ϕ (CSD) and ψ (CSD) in **2**, −29° (25°) and 20° (22°); in **3**, −36° (36°) and 8° (27°); in **4**, −37° (34°) and 10° (26°); ϕ = H1′−C1′−O1′−CX and ψ = C1′−O1′−CX−HX (CX = aglycone carbon) were compared to histograms obtained from 1 μs aqueous molecular dynamics (MD) simulations and X-ray database statistical analysis. *MA'AT*-derived models of ψ were in very good agreement with the MD and X-ray data, but not those of ϕ, suggesting a need for force field revision. The effect of structural context on linkage conformation was also investigated in four selectively ^{13}C-labeled homomannose tri- and tetrasaccharides using the *MA'AT* method. In the cases examined, context effects were found to be small.

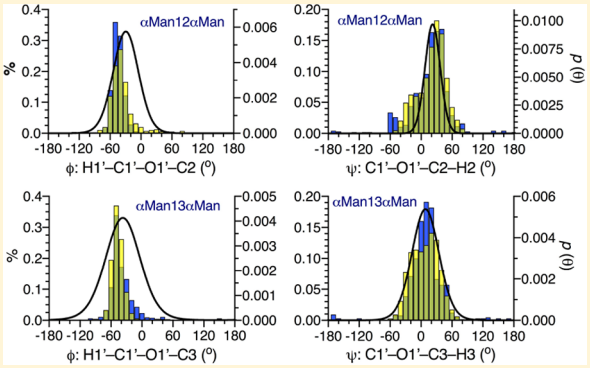

High-mannose oligosaccharides such as **1** are commonly found covalently attached to human glycoproteins,[1−5] including CD2, a T-cell-specific surface adhesion receptor protein that mediates the regulatory and effector functions of T lymphocytes.[6,7] *N*-Glycan **1** appears to be important in maintaining the native conformation of CD2 and directly mediates its interaction with CD58 on antigen-presenting cells.[8] The binding affinities of saccharides to glycoprotein receptors like CD2 are affected by saccharide conformational equilibria and kinetics on the protein,[9] and efforts to characterize these properties are considered essential to arriving at a full understanding of the biological properties of these important biomolecules. While oligosaccharides such as **1** contain multiple conformational domains,[10] their overall shapes are largely determined by the behavior of their constituent *O*-glycosidic linkages, thus explaining ongoing efforts to characterize these linkages in oligosaccharides free in solution, appended to proteins, or bound to receptors.

Current NMR-based approaches to evaluate oligosaccharide conformation, either free in solution or bound to receptors, are confined mainly to the measurement and analysis of inter-residue ^{1}H−^{1}H NOEs or ROEs, and to residual dipolar couplings (RDCs).[11,12] However, these parameters do not provide an unequivocal determination of preferred linkage conformation, in part due to their low abundance in many oligosaccharides and/or to their nonlinear averaging in the presence of conformational exchange. One solution to this problem involves the measurement of multiple and redundant NMR *J*-couplings across *O*-glycosidic linkages in suitably ^{13}C-labeled samples.[13−15] For saccharides of modest size, NMR spin−spin coupling constants (*J*-couplings) are valuable experimental parameters to investigate conformational properties in the presence of motional averaging because of their high

Received: October 4, 2018
Revised: January 3, 2019
Published: January 3, 2019

DOI: 10.1021/acs.biochem.8b01050
Biochemistry 2019, 58, 546−560

abundance and the fact that they average linearly.[16−19] To use these *J*-couplings quantitatively, however, relationships correlating their magnitudes and signs with one or more molecular parameters such as a torsion angle must be available; in this and prior work, these equations were obtained from density functional theory (DFT) calculations fit to a modified form of the Karplus equation.[20] Circular statistics can then be applied to treat the multiple, redundant *J*-couplings (i.e., those sensitive to the same torsion angle) to derive conformational models of the angle.[15,21] The power of this approach was demonstrated in recent studies of the phi (ϕ) and psi (ψ) torsion angles in various β-(1→4) *O*-glycosidic linkages.[15] In this prior work, ensembles of *J*-couplings ($^2J_{COC}$, $^3J_{COCH}$, $^3J_{COCC}$) sensitive to ϕ and ψ were analyzed using DFT-parameterized equations, Fredholm theory, and circular statistics to derive experiment-based rotamer populations for each angle. The conformational models of ϕ and ψ were found to be in very good agreement with those predicted from 1 μs aqueous molecular dynamics (MD) simulations, providing reliable evidence that conformational models can be obtained by NMR for mobile domains in saccharides, such as *O*-glycosidic linkages, with minimal input from theory.

High-mannose *N*-glycan **1** contains seven different types of *O*-glycosidic linkages (αMan-(1→2)-αMan, αMan-(1→3)-αMan, αMan-(1→3)-βMan, βGlcNAc-(1→4)-βGlcNAc, βMan-(1→4)-βGlcNAc, αMan-(1→6)-αMan, and αMan-(1→6)-βMan) and one *N*-glycosidic linkage (βGlcNAc-(1→N$^{\gamma}$)-Asn) (Scheme 1). The long-range research goal of this laboratory is to determine the conformational properties of each of these linkages in isolation, that is, in simple disaccharides or monosaccharide-amino acid adducts in which structural factors controlling these properties are limited in number and are short-range. The properties of these "reference states" are then compared to those of the same linkages embedded in larger oligosaccharides, thereby exposing context effects that are presumably determined by more numerous and/or longer-range structural factors (e.g., steric crowding, H-bonding, other noncovalent interactions, solvation effects). An example of this comparison is illustrated in Scheme 2. The seven different *O*-glycosidic linkages in **1** can be classified into two-bond and three-bond linkages.[15] Prior work treated the two-bond β-(1→4) linkages in **1**;[15] this report focuses on the remaining two-bond αMan-(1→2)-αMan, αMan-(1→3)-αMan, and αMan(1→3)-βMan linkages (Scheme 3). Upcoming reports will treat the three-bond αMan-(1→6)-αMan and αMan-(1→6)-βMan linkages and the *N*-glycosidic linkage in βGlcNAc-(1→N$^{\gamma}$)-Asn.

Scheme 1. Structure of *N*-Glycan 1 and Its Breakdown into Eight Unique *O*- and *N*-Glycosidic Linkages, Each Representing a Reference State for Use in Studies of the Effects of Context on Linkage Properties (See Text)

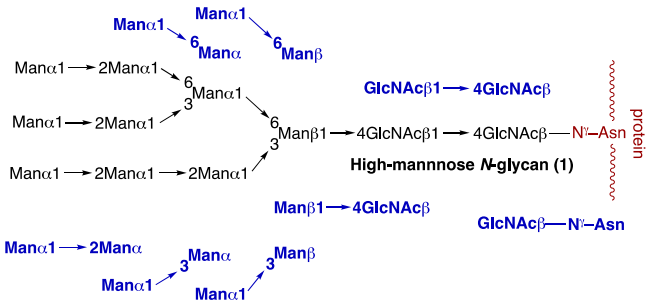

Scheme 2. Hypothetical Context Effect on the αMan-(1→6)-βMan Linkage in 1 (Highlighted in Blue) Caused by a Remote (Long-Range) and Persistent H-Bonding Interaction between O6 of Residue 6″ and an OH Group (Serine Side-Chain) on a Glycoprotein[a]

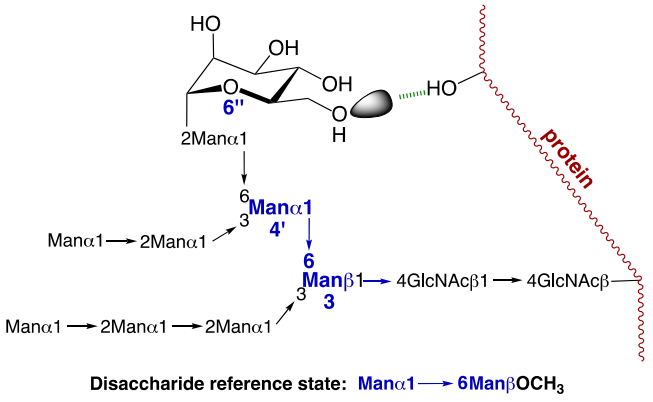

[a]This effect can be detected and quantified by comparing its behavior to that of the (1→6)-linkage in the disaccharide reference state, αMan-(1→6)-βManOCH$_3$.

Scheme 3. Man-Man Disaccharide Reference States 2−4 Investigated in This Study[a]

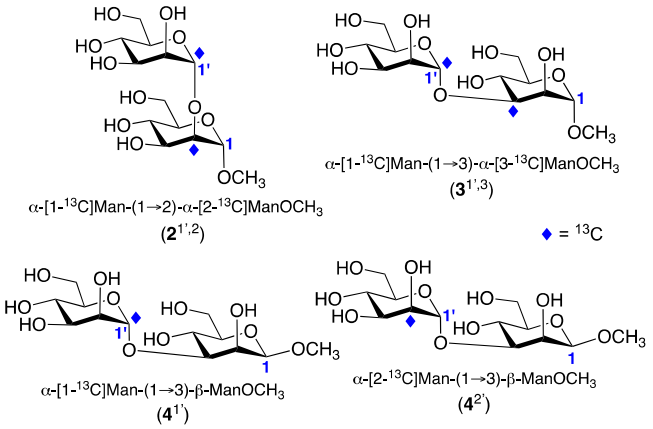

[a]The superscripts identify the carbon atoms in each compound that were labeled with ^{13}C (e.g., **2**$^{1',2}$ is a doubly ^{13}C-labeled isotopomer of **2** containing 99 atom % ^{13}C at C2 and C1′).

In this report, three Man-Man disaccharides were prepared with selective ^{13}C-enrichment to enable measurements of J_{CH} and J_{CC} values across their internal *O*-glycosidic linkages: αMan-(1→2)-αManOCH$_3$ (**2**), αMan-(1→3)-αManOCH$_3$ (**3**) and αMan-(1→3)-βManOCH$_3$ (**4**) (Scheme 3). These disaccharides were prepared as methyl glycosides on their "reducing ends" to eliminate signal multiplicities caused by the presence of anomeric pairs, which can complicate ^{1}H and ^{13}C NMR spectral analysis (see Figure S3 in the Supporting Information of ref 15). The ^{13}C-labeling patterns in **2**−**4** were optimized to measure conventional *J*-values across *O*-glycosidic linkages, as discussed in prior work.[15,18] The redundant *J*-values measured in **2**−**4** were then analyzed using the *MA'AT* circular statistics package[15] to model the ϕ and ψ torsion angles in their linkages, and these models were compared to those obtained from aqueous 1 μs MD simulations. To begin

DOI: 10.1021/acs.biochem.8b01050
Biochemistry 2019, 58, 546−560

assessing the effects of context on αMan-(1→2)-αMan and αMan-(1→3)-α/βMan linkages in higher order structures, four oligosaccharides **5**–**8** (Scheme 4) were prepared with selective ^{13}C-enrichment to allow direct comparison of *trans*-glycoside *J*-coupling ensembles in **5**–**8** to corresponding ensembles in reference disaccharides **2**–**4**.

Scheme 4. High-Mannose Oligosaccharides 5–8 Containing αMan-(1→2)-αMan and αMan-(1→3)-α/βMan *O*-Glycosidic Linkages Used To Evaluate the Effect of Context on Linkage Conformation[a]

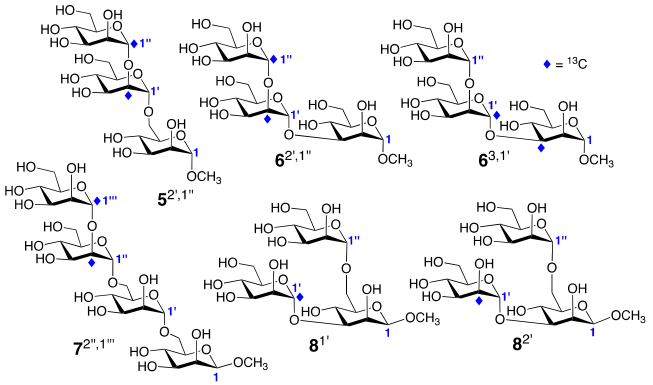

[a]See Scheme 3 for definitions of the superscripts in the compound numbers.

EXPERIMENTAL SECTION

Preparation of ^{13}C-Labeled Oligosaccharides 2–8. ^{13}C-Labeled oligosaccharides **2**–**8** were prepared from D-[1-^{13}C]mannose, D-[2-^{13}C]mannose, and/or D-[3-^{13}C]-mannose; the singly ^{13}C-labeled monosaccharides were prepared by cyanohydrin reduction and/or molybdate-catalyzed epimerization (Scheme 5).[22−24] αMan-(1→2)-

Scheme 5. General Chemical Routes Used To Prepare D-[1-^{13}C]Mannose, D-[2-^{13}C]Mannose, and D-[3-^{13}C]Mannose for Incorporation into ^{13}C-Labeled Oligosaccharides 2–8[a]

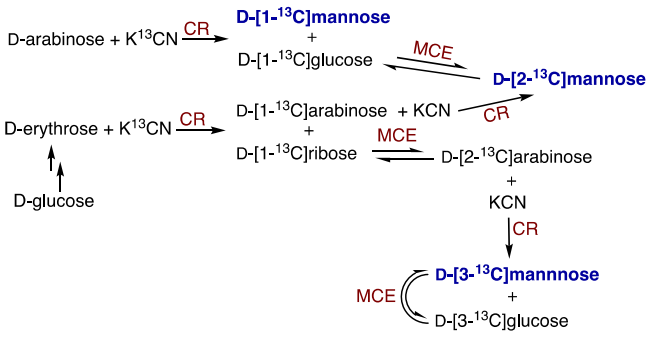

[a]CR = cyanohydrin reduction. MCE = molybdate-catalyzed epimerization. See refs 22–24 for more details.

αManOCH$_3$ (**2**$^{1',2}$) and αMan-(1→3)-[αMan-(1→6)]-βMan-OCH$_3$ (**8**$^{1'}$ and **8**$^{2'}$) were prepared as described previously,[25] and αMan-(1→2)-αMan-(1→6)-αMan-(1→6)-βManOCH$_3$ (**7**$^{2'',1'''}$) was prepared by a minor modification of the chemical route reported previously to prepare a ^{13}C-labeled high-mannose hexasaccharide.[26] Synthetic protocols to prepare ^{13}C-labeled αMan-(1→2)-αManOCH$_3$ (**2**$^{1',2'}$), αMan-(1→3)-αManOCH$_3$ (**3**$^{1',3}$), αMan-(1→3)-βManOCH$_3$ (**4**$^{1'}$ and **4**$^{2'}$), αMan-(1→2)-αMan-(1→6)-αManOCH$_3$ (**5**$^{2',1''}$), and αMan-(1→2)-αMan-(1→3)-αManOCH$_3$ (**6**$^{2',1''}$ and **6**$^{3,1'}$) are provided in the Supporting Information. See Schemes 3 and 4 for explanations of the superscripts used to identify the ^{13}C-labeled carbons in **2**–**8**.

NMR Spectroscopy. High-resolution 1D ^{1}H and ^{13}C{^{1}H} NMR spectra were obtained using 5 mm NMR tubes on a 600 MHz FT-NMR spectrometer equipped with a 5 mm ^{1}H–^{19}F/^{15}N–^{31}P AutoX dual broadband probe. NMR spectra of synthetic intermediates were collected in $CDCl_3$ at 22 °C. ^{1}H NMR spectra (600 MHz) were collected with an ∼6000 Hz spectral window and an ∼4.0 s recycle time, and ^{13}C{^{1}H} NMR spectra (150 MHz) were collected with an ∼30,000 Hz spectral window and ∼3.0 s recycle time. ^{1}H and ^{13}C Chemical shifts were referenced internally to the residual $CHCl_3$ signal in the $CDCl_3$ solvent.

High-resolution ^{1}H and ^{13}C{^{1}H} NMR spectra of ^{13}C-labeled **2**–**8** (Schemes 3 and 4) were obtained on ∼20 and ∼100 mM aqueous (^2H_2O) solutions, respectively, at 22 °C. ^{1}H NMR spectra were collected with an ∼2800 Hz spectral window and ∼4 s recycle time, and FIDs were zero-filled to give final digital resolutions of <0.01 Hz/pt. ^{13}C{^{1}H} NMR spectra were collected with an ∼12,800 Hz spectral window and ∼5 s recycle time, and FIDs were zero-filled to give final digital resolutions of <0.05 Hz/pt. FIDs were processed with resolution enhancement (Gaussian or sine-bell functions) to improve resolution and facilitate the measurement of small *J*-couplings (≥0.5 Hz), and reported *J*-couplings are accurate to ±0.1 Hz, unless otherwise stated (representative NMR spectra of **2**–**8** are shown in Figures S1–S7 in the Supporting Information). Coupling signs for $^2J_{CH}$ and $^2J_{CC}$ values were assigned using empirical projection rules[27,28] and/or are based on signs determined from DFT calculations. To measure $^3J_{C3,H1'}$ values in **4** and **8**, 2D ^{13}C–^{1}H *J*-HMBC spectra[29] were obtained with a two-fold low-pass *J*-filter applied to suppress $^1J_{CH}$ values. A discussion of potential non-first-order effects on the measurement of *trans*-glycosidic J_{CH} and J_{CC} values is provided in the Supporting Information.

COMPUTATIONS

Geometric Optimization of Model Disaccharides 2–4. Density functional theory (DFT) calculations were conducted on model disaccharides **2**^{c}, **3**^{c}, and **4**^{c} (the "c" superscript denotes *in silico* structures) within *Gaussian09*[30] using the B3LYP functional[31] and 6-31G* basis set[32] for geometric optimization. The effects of solvent water were treated using the self-consistent reaction field (SCRF)[33] and the integral equation formalism (polarizable continuum) model (IEFPCM).[34] Exocyclic C–C and C–O torsion angles in **2**^{c}–**4**^{c} were constrained as described in Scheme S1 (Supporting Information); only one set of these angles was investigated at each incremented value of ϕ and ψ. These torsional constraints were imposed to simplify geometric optimizations and acquire only the heavy atom geometric information on ϕ/ψ that is needed to parameterize *J*-coupling equations, resulting in a restricted energetic landscape that may not be reflective of the total landscape. Consequently, preferred geometries about ϕ and ψ in **2**–**4** predicted from an inspection of the potential energy surfaces are prone to

DOI: 10.1021/acs.biochem.8b01050
Biochemistry 2019, 58, 546–560

error, although the data can identify general regions of ϕ/ψ space that are likely to be more occupied than others. Torsion angles phi (ϕ = H1′−C1′−O2−C2 for $\mathbf{2}^c$; ϕ = H1′−C1′−O3−C3 for $\mathbf{3}^c$ and $\mathbf{4}^c$) and psi (ψ = C1′−O2−C2−H2 for $\mathbf{2}^c$; ψ = C1′−O3−C3−H3 for $\mathbf{3}^c$ and $\mathbf{4}^c$) were varied in 15° increments through 360° and held constant during geometry optimization, yielding 576 final structures of each model disaccharide.

DFT Calculations of NMR Spin-Coupling Constants in Disaccharides $\mathbf{2}^c$−$\mathbf{4}^c$. J_{HH}, J_{CH}, and J_{CC} values were calculated in each geometry-optimized structure of $\mathbf{2}^c$−$\mathbf{4}^c$ using DFT and the B3LYP functional[31] in *Gaussian09*.[30] The Fermi contact,[35−37] diamagnetic and paramagnetic spin−orbit, and spin−dipole terms[35] were recovered using a specially designed basis set, [5s2p1d|3s1p],[19,38] and raw (unscaled) calculated couplings are reported and are accurate to within ±0.2−0.3 Hz based on prior work.[38] The self-consistent reaction field (SCRF)[33] and the integral equation formalism (polarizable continuum) model (IEFPCM)[34] were used to treat the effects of solvent water during the *J*-coupling calculations. Plots of DFT-calculated *J*-couplings vs ϕ or ψ were generated using the graphics software, *Prism*.[39] Three *J*-couplings were used to model ϕ and three *J*-couplings were used to model ψ in **2**−**4** (Scheme 6).

Scheme 6. Redundant J_{CH} and J_{CC} Values Sensitive to the Phi (ϕ) and Psi (ψ) Torsion Angles in the α-(1→2) and α-(1→3) Linkages of 2 and 3−4, Respectively[a]

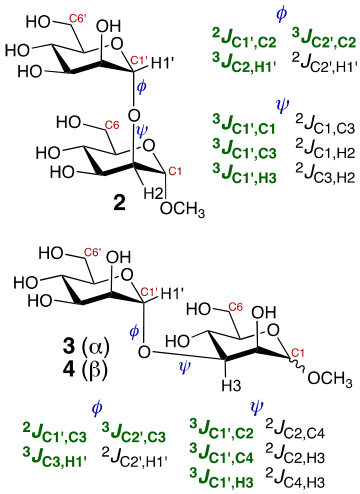

[a]Six conventional *J*-values shown in green were parameterized and used to model ϕ and ψ in **2**−**4**. Unconventional *J*-values sensitive to ϕ and ψ are also shown (black) but were not used in this study.

Parameterization of *J*-Coupling Equations For α-(1→2)- and α-(1→3)-Linkages in $\mathbf{2}^c$−$\mathbf{4}^c$. Equations relating six DFT-calculated *J*-couplings to either ϕ or ψ in $\mathbf{2}^c$−$\mathbf{4}^c$ were parameterized using the scipy and numpy packages in Python[40] to give modified Karplus-like equations[20] of the form shown in eq A. Equations were parameterized using a subpopulation

$$^xJ_{ab}(\mathrm{Hz}) = A + B\cos(\theta) + C\sin(\theta) + D\cos(2\theta) + E\sin(2\theta) \quad \text{(A)}$$

of conformers that was selected using an energy cutoff to remove sterically strained conformers.[15] The goodness-of-fit of each equation is reported as a root mean squared (RMS) deviation.

Determinations of *O*-Glycosidic Linkage Conformational Models for 2−8 Using NMR *J*-Coupling Ensembles and *MA'AT*. NMR *J*-coupling ensembles (three experimental values each for ϕ and ψ; Scheme 6) and DFT-parameterized equations were combined with Fredholm theory and circular statistics to determine conformational populations of the α-(1→2) and/or α-(1→3) linkages in **2**−**8**, (Schemes 3 and 4) using the statistical software, *MA'AT*.[15,20] Users can access the current version of *MA'AT* at the Serianni laboratory online data archive: www3.nd.edu/~aserilab. Username and password information that is needed to gain access to this Web site can be obtained by contacting the Serianni laboratory. A manuscript describing the *MA'AT* program and a users manual are in preparation.

Linkage torsion angles, ϕ and ψ, were modeled as a single von Mises distribution, which yields two fitting parameters, the mean position and the circular standard deviation (CSD) of ϕ or ψ.[15] Monte Carlo methods were used to generate model parameters, and least-squares methods were used to minimize the RMS deviation between the experimental and predicted *J*-couplings. The mean position and CSD of each model were calculated using the circular statistics package in *R*.[41,42] Approximate standard errors for the model parameters were computed by taking the square root of the diagonal elements from the estimated covariance matrix.[42]

Two- and three-state models of ϕ and ψ can be tested using the *MA'AT* software for two-bond *O*-glycosidic linkages such as those found in **2**−**8**, but these treatments require more experimental restraints than used in this work. Nonconventional *J*-couplings sensitive to ϕ and ψ (Scheme 6) could provide additional constraints. NOEs,[43,44] residual dipolar couplings (RDCs)[12,46,47] and/or residual chemical shift anisotropies (RCSAs)[48,49] are additional NMR parameters that might allow more complex models and distributions of ϕ and ψ to be tested in the future.

Molecular Dynamics Simulations of Disaccharides 2−4 and Tetrasaccharide 7. Initial structures of **2**−**4** and **7** (Schemes 3 and 4) were built using the Carbohydrate Builder module available at the GLYCAM Web site (http://www.glycam.org).[50] The GLYCAM06[51] (version j) force field was employed in all simulations. Structures **2**−**4** and **7** were solvated with TIP3P[52] water using a 12 Å buffer in a cubic box, using the LEaP module in the *AMBER14* software package.[53] Energy minimizations for solvated **2**−**4** and **7** were performed separately under constant volume (500 steps steepest descent, followed by 24,500 steps of conjugate-gradient minimization). Each system was subsequently heated to 300 K over a period of 50 ps, followed by equilibration at 300 K for a further 0.5 ns using the nPT condition, with the Berendsen thermostat[54] for temperature control. All covalent bonds involving hydrogen atoms were constrained using the SHAKE algorithm,[55] allowing a simulation time step of 2 fs throughout the simulation. After equilibration, production simulations were carried out with the GPU implementation[56] of the PMEMD.MPI module, and trajectory frames were collected every 1 ps for a total of 1 μs. One to four nonbonded interactions were not scaled[57] and a nonbonded cutoff of 8 Å was applied to van der Waals interactions, with long-range electrostatics treated with the particle mesh Ewald approximation. Output from each MD simulation was imported into *Prism* for visualization.

DOI: 10.1021/acs.biochem.8b01050
Biochemistry 2019, 58, 546−560

Table 1. Trans-glycoside NMR *J*-Couplings in Compounds Containing an αMan-(1→2)-αMan Glycosidic Linkage[a]

compd	ϕ-dependent *J*-couplings			ψ-dependent *J*-couplings		
	$^{2}J_{C1',C2}$	$^{3}J_{C2',C2}$	$^{3}J_{C2,H1'}$	$^{3}J_{C1',C1}$	$^{3}J_{C1',C3}$	$^{3}J_{C1',H2}$
αMan-(1→2)-αManOCH$_3$ (**2**)	−1.8	3.6	4.2	br	2.0	4.6
αMan-(1→2)-αMan-(1→6)-αManOCH$_3$ (**5**)	−1.7	3.5	4.0	br	1.6	4.6
αMan-(1→2)-αMan-(1→3)-αManOCH$_3$ (**6**)	−1.8	3.6	3.9	br	1.7	4.5
αMan-(1→2)-αMan-(1→6)-αMan-(1→6)-βManOCH$_3$ (**7**)	−1.7		3.9	br		4.5
average values (STD)[b]	−1.8 (0.1)	3.6 (0.1)	4.0 (0.1)	br	1.8 (0.2)	4.6 (0.1)

[a]In Hz ± 0.1 Hz; 22 °C; in $^{2}H_2O$; br denotes broadened signal (J < 0.5 Hz). [b]STD = standard deviation; shown in parentheses. All ^{3}J values are assumed to be positive in sign.

Table 2. Trans-glycoside NMR *J*-Couplings in Compounds Containing an αMan-(1→3)-α/βMan Glycosidic Linkage[a]

compd	ϕ-dependent *J*-couplings			ψ-dependent *J*-couplings		
	$^{2}J_{C1',C3}$	$^{3}J_{C2',C3}$	$^{3}J_{C3,H1'}$	$^{3}J_{C1',C2}$	$^{3}J_{C1',C4}$	$^{3}J_{C1',H3}$
αMan-(1→3)-αManOCH$_3$ (**3**)	−1.8	3.4	3.6	br	1.4	4.9
αMan-(1→3)-βManOCH$_3$ (**4**)	−1.9	3.5	3.7	br	1.5	4.9
αMan-(1→2)-**αMan(1→3)-αMan**OCH$_3$ (**6**)	−1.7	3.5	3.7	br	1.4	4.8
αMan-(1→3)[αMan-(1→6)]-**βMan**OCH$_3$ (**8**)	−1.8	3.6	3.8	br	1.5	4.9
average values (STD)[b]	−1.8 (0.1)	3.5 (0.1)	3.7 (0.1)	br	1.5 (0.1)	4.9 (0.1)

[a]In Hz ± 0.1 Hz; 22 °C; in $^{2}H_2O$; br denotes broadened signal (J < 0.5 Hz). [b]STD = standard deviation, shown in parentheses. All ^{3}J values are assumed to be positive in sign.

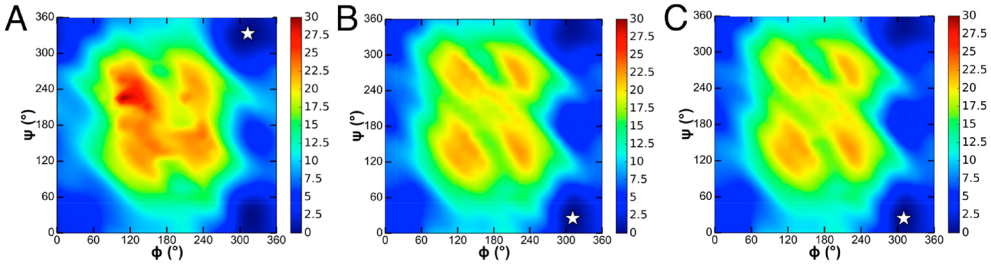

Figure 1. DFT-derived potential energy surfaces (PES) for αMan-(1→2)-αManOCH$_3$ **2** (A), αMan-(1→3)-αManOCH$_3$ **3** (B), and αMan-(1→3)-βManOCH$_3$ **4** (C). The global energy minimum is identified by the star on each PES map. Energy units on the right-hand axes are in kcal/mol. As discussed in the text, these maps are not quantitative since they were generated from very limited sampling of the conformational space.

RESULTS AND DISCUSSION

Qualitative Comparisons of ϕ- and ψ-Dependent *J*-Coupling Ensembles in 2−8. NMR *J*-couplings sensitive to the internal *O*-glycosidic linkage conformations in **2**−**8** were measured in aqueous ($^{2}H_2O$) solution (Tables 1 and 2; see representative NMR spectra in Figures S1−S7, Supporting Information). The αMan-(1→2)-αMan linkages in disaccharide **2** and oligosaccharides **5**−**7** give essentially identical ensembles of ϕ-dependent *J*-couplings (Table 1), from which the following average *J*-couplings with their standard deviations were calculated: $^{2}J_{C1',C2}$ = −1.8 ± 0.1 Hz, $^{3}J_{C2',C2}$ = 3.6 ± 0.1 Hz, and $^{3}J_{C2,H1'}$ = 4.0 ± 0.1 Hz (Table 1). The standard deviations lie within the experimental errors of the measurements, indicating that the differences are statistically insignificant. Similar but not identical ensembles of ψ-dependent *J*-couplings for the αMan-(1→2)-αMan linkages in **2** and **5**−**7** were observed, from which the following average values with their standard deviations were calculated (Table 1): $^{3}J_{C1',C1}$ = br; $^{3}J_{C1',C3}$ = 1.8 ± 0.2 Hz; $^{3}J_{C1',H2}$ = 4.6 ± 0.1 Hz. The standard deviation for $^{3}J_{C1',C3}$ exceeds 0.1 Hz, indicating statistically significant differences, but line-broadening of the C1 signal when C1′ is ^{13}C-labeled precludes a determination of whether the $^{3}J_{C1',C1}$ values also differ statistically. Nevertheless, these findings indicate qualitatively that the conformation of a terminal αMan-(1→2)-αMan linkage is not affected significantly when the disaccharide bearing that linkage serves as a donor to one or two αMan residues to give a linear (unbranched) tri- (**6**) or tetrasaccharide (**7**), respectively.

Corresponding ensembles of *J*-couplings sensitive to ϕ and ψ are virtually identical for the αMan-(1→3) linkages in αMan-(1→3)-αManOCH$_3$ (**3**) and αMan-(1→3)-βManOCH$_3$ (**4**), suggesting that configuration at the anomeric carbon of the "reducing" terminal Man residue (i.e., that bearing the OCH$_3$ aglycone) does not affect the conformational properties of the α-(1→3) linkage appreciably (Table 2). Neither α-mannosylation at O2 of the "non-reducing" terminal αMan residue of **3** to give unbranched trisaccharide **6**, nor α-mannosylation at O6 of the βMan residue of **4** to give branched trisaccharide **8**, affect the conformational properties of the α-(1→3) linkage; the ensembles of *J*-couplings sensitive to ϕ and ψ in disaccharides **3** and **4** are virtually identical to corresponding ensembles in trisaccharides **6** and **8**, respectively. Averaging the ϕ- and ψ-dependent *J*-couplings for the four αMan-(1→3) linkages in **3**, **4**, **6** and **8** gave standard deviations within the experimental error of the measurements (±0.1 Hz): for ϕ, $^{2}J_{C1',C3}$ = −1.8 ± 0.1 Hz, $^{3}J_{C2',C3}$ = 3.5 ± 0.1 Hz, $^{3}J_{C3,H1'}$ = 3.7 ± 0.1 Hz; for ψ, $^{3}J_{C1',C2}$ < 0.5 Hz, $^{3}J_{C1',C4}$ = 1.5 ± 0.1 Hz, $^{3}J_{C1',H3}$ = 4.9 ± 0.1 Hz (Table 2).

The qualitative comparisons made above hinge on the assumption that the equations relating a given ensemble of *J*-

DOI: 10.1021/acs.biochem.8b01050
Biochemistry 2019, 58, 546−560

couplings to either ϕ or ψ are the same for all linkages; for example, in the comparison of *J*-values in disaccharides **3** and **4** (Table 2), the equations relating the six *J*-couplings to either ϕ or ψ are assumed to be unaffected by configuration at C1 of the "reducing" Man residue. In all cases but one, this assumption is probably valid given the terminal locations of the αMan-(1→2)-αMan linkages in **2** and **5**−**7** (Table 1), and the terminal locations of the αMan-(1→3)-α/βMan linkages in **3**, **4** and **8** (Table 2). The one possible exception is trisaccharide **6**, since the αMan residue participating in the αMan-(1→3)-αMan linkage is α-mannosylated at O2, thus possibly affecting the equation relating $^3J_{C2',C3}$ to ϕ. Since this potential substitution effect is absent in **3**, **4**, and **8**, the validity of directly comparing $^3J_{C2',C3}$ values in all four αMan-(1→3)-α/βMan linkages might be called into question. However, the data indicate that this effect, if present, is probably small (the 3.5 Hz value in **6** is very similar to the remaining three $^3J_{C2',C3}$ values), and key secondary factors influencing $^3J_{C2',C3}$ remain intact in **6** (i.e., the identity of the terminal electronegative oxygen substituent at C2′ and its axial orientation are identical to those in **3**, **4**, and **8**).[13,18,58]

Preferred Linkage Conformations in Disaccharides 2−4 Determined from DFT-Derived Potential Energy Surfaces. DFT-Derived potential energy surfaces (PESs) for disaccharides **2**−**4** are shown in Figure 1. As discussed above, these maps were derived from a limited survey of the conformational space available to **2**−**4**, and thus preferred geometries about ϕ and ψ in **2**−**4** predicted from them are prone to error. Linkage conformers associated with the global energy minimum of these plots were as follows: for **2**, ϕ = 312°, ψ = 332°; for **3**, ϕ = 311°, ψ = 25°; for **4**, ϕ = 310°, ψ = 24°. In these conformers, ϕ assumes a value of ∼315°, which orients the aglycone carbon nearly antiperiplanar to C2′. This geometry is expected to be preferred based on stereoelectronic considerations[59−67] (*exo*-anomeric effect). The nearly identical PES maps for **3** and **4** (Figure 1) indicate that configuration at the anomeric carbon bearing the OCH_3 aglycone does not significantly affect the conformational behavior of the α-(1→3) linkage, consistent with the conclusions drawn from qualitative analysis of the trans-glycoside *J*-couplings in **3** and **4** (see section above).

The PES maps for disaccharides **2**−**4** show energy minima for ψ at ∼30°, ∼180°, and ∼330°. The global energy minimum appears at ψ = ∼330° for **2**, and ψ = ∼30° for **3** and **4**. However, in each case, the energy difference between conformers having ∼30° and ∼330° values of ψ is <1 kcal/mol, and the conformer with ψ near 180° is only ∼5 kcal/mol higher in energy than the global minimum. Given these small energy differences, assignments of preferred ψ torsion angles in **2**−**4** cannot be made with confidence based solely on PES data. The greater uniformity of ϕ, relative to ψ, suggests that the former may be more conformationally constrained in **2**−**4**. However, as discussed above, the PES data were collected over a small fraction of the energy hypersurface, that is, only a very small subset of exocyclic torsion angles was sampled in the DFT calculations (Scheme S1, Supporting Information). Thus, while the PES results provide useful clues about the preferred regions of ϕ/ψ space, reliable determinations of the preferred values of ϕ and ψ in **2**−**4** cannot be made with confidence from these data.

Structural Dependencies of ϕ- and ψ-Dependent *J*-Couplings in Disaccharides 2−4. Equations were parameterized for the six conventional ϕ- and ψ-dependent *J*-couplings in **2**−**4** (*J*-values shown in green in Scheme 6), giving a total of 18 parameterized equations (ϕ/ψ hypersurfaces for these *J*-couplings are shown in Figures S8 and S9, Supporting Information). Equations that were very similar for the three linkages in **2**−**4** were combined to give a single generalized equation (the individual equations for each *J*-coupling in **2**−**4** are available in the Serianni Laboratory Data Archive: https://www3.nd.edu/~aserilab/Disaccharide_Database/Home/DATA.html).

Three-Bond (Vicinal) $^{13}C-^1H$ Spin-Couplings − $^3J_{COCH}$. 2D Contour plots of DFT-calculated trans-glycosidic $^3J_{COCH}$ values in **2** and **3** exhibit a dynamic range of ∼10 Hz (Figure 2).

$$^3J_{COCH}\ (\text{Hz}) = 4.04 - 1.72\cos(\theta) + 0.18\sin(\theta) + 3.70\cos(2\theta) - 0.91\sin(2\theta) \quad \text{rms} = 0.72\ \text{Hz} \qquad (1)$$

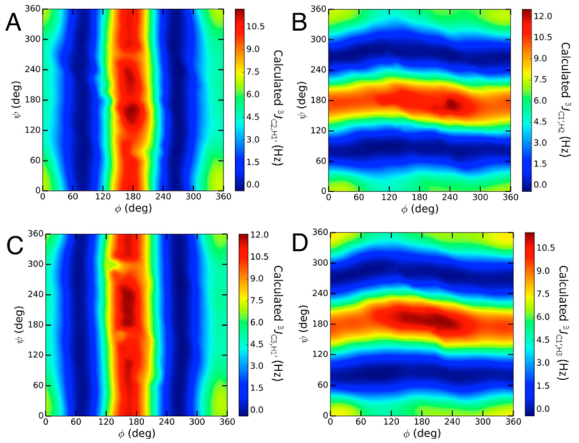

Figure 2. Contour plots of calculated $^3J_{COCH}$ values in **2** and **3**. (A) $^3J_{C2,H1'}$ in **2**, showing a primary dependence on ϕ. (B) $^3J_{C1',H2}$ in **2**, showing a primary dependence on ψ. (C) $^3J_{C3,H1'}$ in **3**, showing a primary dependence on ϕ. (D) $^3J_{C1',H3}$ in **3**, showing a primary dependence on ψ.

$^3J_{C2,H1'}$ is essentially unaffected by ψ and $^3J_{C1',H2}$ is essentially unaffected by ϕ for the αMan-(1→2)-αMan linkage in **2** (Figure 2A and B). Similarly, $^3J_{C3,H1'}$ is essentially unaffected by ψ and $^3J_{C1',H3}$ is essentially unaffected by ϕ for the αMan-(1→3)-αMan linkage in **3** (Figure 2C and D). The six parameterized $^3J_{COCH}$ equations for **2**−**4** show very similar dependencies of $^3J_{COCH}$ on the C−O−C−H torsion angle, indicating behavior that is largely independent of the linkage type (Figure 3). Consequently, the six parameterized equations were combined to give a single generalized equation (eq 1)

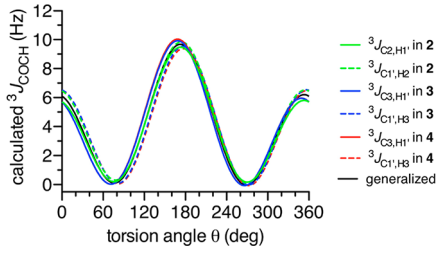

Figure 3. Plots of calculated trans-glycoside $^3J_{COCH}$ values in disaccharides **2**−**4** as a function of torsion angle θ, where θ is either ϕ or ψ (see text). The curve shown in black corresponds to generalized eq 1.

DOI: 10.1021/acs.biochem.8b01050
Biochemistry 2019, 58, 546−560

which was used to treat $^{3}J_{COCH}$ values in **2**−**4** (in eq 1, θ denotes either ϕ or ψ depending on the specific $^{3}J_{COCH}$ value).

A comparison of eq 1 with that obtained previously for β-(1→4)-linked disaccharides[15] shows no significant difference, providing additional justification for the use of a generalized equation to treat trans-glycoside $^{3}J_{COCH}$ values across different *O*-glycosidic linkages. Exceptions, however, may exist, such as when the coupled carbon is bonded to an ionizable substituent (e.g., ψ-dependent $^{3}J_{C2,HX}$ values involving *N*-acetyl-neuraminic acid which bears a COOH group attached to C2). In the latter case, not only might the curve differ in amplitude and/or phase, but it may also depend on the state of COOH ionization.

Two-Bond (Geminal) ^{13}C−^{13}C Spin-Coupling − $^{2}J_{COC}$. Geminal $^{2}J_{COC}$ values across *O*-glycosidic linkages show a primary dependence on ϕ and a secondary dependence on ψ.[18,68] This behavior is responsible for the more complex 2D contour plots of $^{2}J_{C1',C2}$ vs ϕ/ψ in **2** and

$$^{2}J_{C1',C2}\ (\text{Hz}) = -2.56 + 0.93\cos(\phi) + 0.34\sin(\phi) - 0.35\cos(2\phi) + 0.42\sin(2\phi) \quad \text{rms} = 0.68\ \text{Hz} \qquad (2)$$

$$^{2}J_{C1',C3}\ (\text{Hz}) = -2.79 + 1.15\cos(\phi) + 0.10\sin(\phi) - 0.17\cos(2\phi) + 0.47\sin(2\phi) \quad \text{rms} = 0.53\ \text{Hz} \qquad (3)$$

$^{2}J_{C1',C3}$ vs ϕ/ψ in **3** and **4**, as illustrated in Figure 4 for the αMan-(1→2)-αMan linkage in **2**. In this work, $^{2}J_{COC}$ was parameterized as shown in Figure 5, with each curve representing the average of 24 curves at different ψ values to capture the secondary effects of ψ. Trans-glycoside $^{2}J_{COC}$ values are negative in sign and exhibit a dynamic range of ∼3 Hz, with the least negative values observed at ϕ = ∼60° (O5′ *anti* to C2 in **2**, and O5′ *anti* to C3 in **3** and **4**). The curves for **3** and **4** are very similar, indicating that anomeric configuration at the "reducing" terminal residue does not much affect the parameterization. The amplitude and phase of the curve for $^{2}J_{C1',C2}$ in **2**, however, differ from those for $^{2}J_{C1',C3}$ in **3** and **4**. Consequently, eq 2 was derived to treat $^{2}J_{C1',C2}$ in **2**, and a generalized equation (eq 3) was derived to treat $^{2}J_{C1',C3}$ in **3** and **4**.

Three-Bond (Vicinal) ^{13}C−^{13}C Spin-Couplings − $^{3}J_{COCC}$. The dependencies of $^{3}J_{C1',C1}$ in **2** and $^{3}J_{C1',C2}$ in **3**−**4** on ψ are shown in Figure 6. The curves for **3** and **4** are essentially coincident, indicating that anomeric configuration of the

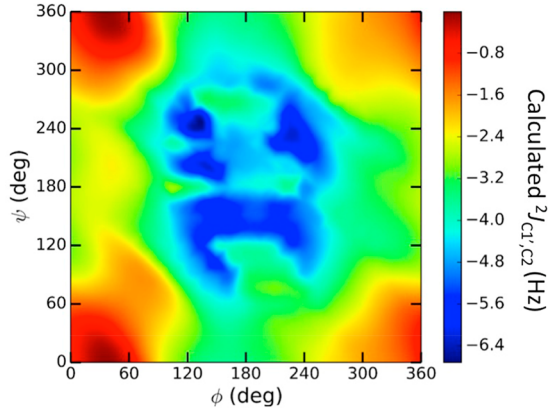

Figure 4. 2D Contour plot showing the dependence of calculated geminal $^{2}J_{C1',C2}$ values in **2** on both ϕ and ψ.

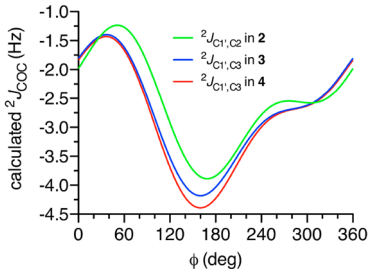

Figure 5. Dependencies of DFT-calculated $^{2}J_{C1',C2}$ and $^{2}J_{C1',C3}$ values in disaccharides **2** and **3**−**4**, respectively, on glycosidic torsion angle ϕ.

"reducing" terminal Man residue does not affect the behavior of $^{3}J_{C1',C2}$, justifying the use of a generalized equation (eq 4) to treat $^{3}J_{C1',C2}$ in both disaccharides. The curve for $^{3}J_{C1',C1}$ in **2** has identical phase to those for $^{3}J_{C1',C2}$ in **3** and **4**, but curve amplitude differs significantly, with calculated *J*-couplings at ψ = 120° and 300° being ∼2 Hz larger than those for **3** and **4** (Figure 6). At ψ = 300°, the coupled carbons, C1′ and C1, adopt an *anti* orientation, producing a planar zigzag arrangement along the C1′−O2−C2−C1−O1 pathway. In this arrangement, a terminal electronegative substituent (O1) lies in the coupling plane and enhances $^{3}J_{C1',C1}$ relative to *anti* orientations devoid of this substituent.[13,18,69,70] The latter pathway geometry pertains to $^{3}J_{C1',C2}$ in **3** and **4** for C1′−O3−C3−C2 coupling pathways at ψ = 300° (Figure 6), but in these cases the terminal substituent atom (C1) is not electronegative and does not affect $^{3}J_{C1',C2}$ magnitude significantly. An enhancement is also observed in $^{3}J_{C1',C1}$ in **2** relative to $^{3}J_{C1',C2}$ in **3** and **4** at ψ = 120° (Figure 6). In **2**, C1′ and C2 are eclipsed with O1 lying in the coupling plane, but the enhancement is smaller relative to that at ψ = 300° since the C1′−O2−C2−C1−O1 pathway does not have a planar zigzag geometry. Equation 5 was parameterized to treat $^{3}J_{C1',C1}$ values in **2**.

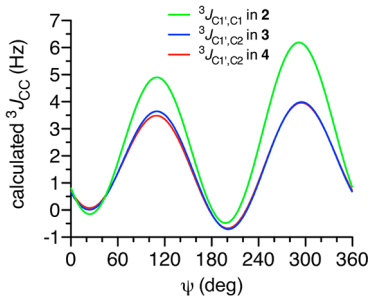

Figure 6. Calculated $^{3}J_{C1',C1}$ values in **2** and $^{3}J_{C1',C2}$ values in **3**−**4** as a function of glycosidic torsion angle ψ.

The dependencies of $^{3}J_{C1',C3}$ on ψ in **2** and $^{3}J_{C1',C4}$ on ψ in **3**−**4** are shown in Figure 7. The C1′−O2−C2−C3 coupling pathway in **2** orients the coupled carbons antiperiplanar at ψ = 60°. In this geometry, the ring oxygen O5′ lies in the C1′−O2−C2−C3 coupling plane at ϕ = 60°, thus accounting for the increased curve amplitude at ψ = 60° relative to that at ψ = 240° where C1′ and C3 are eclipsed. Curve shapes for $^{3}J_{C1',C4}$ in **3** and **4** are identical to that found for $^{3}J_{C1',C3}$ in **2** (Figure 7) but

DOI: 10.1021/acs.biochem.8b01050
Biochemistry 2019, 58, 546−560

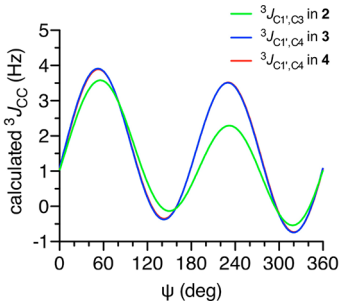

Figure 7. Calculated $^3J_{C1',C3}$ values in **2** and $^3J_{C1',C4}$ values in **3**−**4** as a function of glycosidic torsion angle ψ.

$$^3J_{C1',C2}\ (\text{Hz}) = 1.72 + 0.42\cos(\phi) - 0.05\sin(\phi) - 1.45\cos(2\phi) - 1.43\sin(2\phi) \quad \text{rms} = 0.50\ \text{Hz} \quad (4)$$

$$^3J_{C1',C1}\ (\text{Hz}) = 2.62 + 0.38\cos(\phi) - 0.54\sin(\phi) - 2.18\cos(2\phi) - 1.95\sin(2\phi) \quad \text{rms} = 0.68\ \text{Hz} \quad (5)$$

$$^3J_{C1',C3}\ (\text{Hz}) = 1.31 + 0.21\cos(\psi) + 0.64\sin(\psi) - 0.50\cos(2\psi) + 1.54\sin(2\psi) \quad \text{rms} = 0.35\ \text{Hz} \quad (6)$$

$$^3J_{C1',C4}\ (\text{Hz}) = 1.58 - 0.03\cos(\psi) + 0.27\sin(\psi) - 0.48\cos(2\psi) + 2.07\sin(2\psi) \quad \text{rms} = 0.50\ \text{Hz} \quad (7)$$

show significantly greater amplitudes at $\psi = 240°$; a structural explanation for the latter difference is unclear, but steric compression caused by interactions between O5′ and O4 when C1′ and C4 are eclipsed and $\phi = 300°$ might be responsible. Equation 6 was parameterized to treat $^3J_{C1',C3}$ in **2**, and a generalized equation (eq 7) was parameterized to treat $^3J_{C1',C4}$ in **3** and **4**.

$$^3J_{C2',C2}\ (\text{Hz}) = 2.05 + 0.47\cos(\psi) - 0.55\sin(\psi) - 0.86\cos(2\psi) - 1.92\sin(2\psi) \quad \text{rms} = 0.40\ \text{Hz} \quad (8)$$

$$^3J_{C2',C3}\ (\text{Hz}) = 2.08 + 0.53\cos(\psi) - 0.29\sin(\psi) - 1.11\cos(2\psi) - 2.06\sin(2\psi) \quad \text{rms} = 0.33\ \text{Hz} \quad (9)$$

Similar global maxima were observed for $^3J_{C2',C2}$ in **2** and $^3J_{C2',C3}$ in **3** and **4** at $\phi = 300°$ (Figure 8). At $\phi = 300°$, the coupled carbons are antiperiplanar in **2**−**4**, and the in-plane electronegative terminal O2′ enhances these $^3J_{CCOC}$ values. The C2−O2 bond is axial in **2**, while the C3−O3 bond is

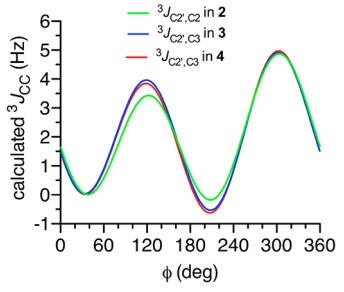

Figure 8. Calculated $^3J_{C2',C2}$ values in **2** and $^3J_{C2',C3}$ values in **3**−**4** as a function of the glycosidic torsion angle ϕ.

equatorial in **3**−**4**, and this difference appears to affect the curves slightly; ∼0.7 Hz differences were observed at $\phi = 120°$ and 210° (Figure 8). Equation 8 was parameterized to treat $^3J_{C2',C2}$ values in **2**. Since configuration of the anomeric carbon in the "reducing" terminal Man residue of **3** and **4** does not affect $^3J_{C2',C3}$ behavior (Figure 8), a generalized equation (eq 9) was obtained to treat $^3J_{C2',C3}$ values in these linkages.

Statistical Modeling of the *O*-Glycosidic Linkages of 2−8. Parameterized *J*-coupling eqs 1−9 and experimental *J*-couplings (Tables 1 and 2) were used to generate single-state von Mises models[15,41] of the rotamer distributions about ϕ and ψ in disaccharides **2**−**4** (Figure 9). The mean positions, circular standard deviations (CSDs) and RMS errors of these models are shown in Table 3. The RMS errors (0.13−0.36 Hz) are relatively small, indicating a good fit of the experimental *J*-couplings to the von Mises model. As expected from the qualitative analysis of the *J*-coupling ensembles (Qualitative Comparisons of ϕ- and ψ-Dependent J-Coupling Ensembles in 2−8), rotamer distributions for ϕ and ψ in **3** and **4** are very similar, confirming that anomeric configuration in the "reducing" terminal Man residue does not significantly affect αMan-(1→3)-Man linkage conformation.

In general, elaboration of reference disaccharides **2** and **3**−**4** to give **5**−**7**, and **6** and **8**, respectively, does not affect the mean values and CSDs for ϕ and ψ significantly. Averaging the data in Table 3 gives the following mean values for ϕ and ψ: in αMan-(1→2)-αMan linkages, $\phi = -31° \pm 12°$, $\psi = 19° \pm 9°$; in αMan-(1→3)-α/βMan linkages, $\phi = -36° \pm 14°$, $\psi = 9° \pm 11°$ (Scheme 7). In both types of linkages, the averaged CSDs are smaller for ψ than for ϕ, indicating greater librational motion about ϕ in both cases. This behavior is consistent with that observed in β-(1→4) linkages, where CSD values were typically larger for ϕ than for ψ.[15] *MA'AT* analysis to date has yielded similar results for ϕ regardless of the configuration of the glycosidic linkage and the identities of the donor and acceptor residues.

The conformational properties of the two types of Man-Man *O*-glycosidic linkages show minor differences. The mean position of ϕ in αMan-(1→2)-αMan linkages (−31°) is ∼5° more positive than the mean position of ϕ found in the αMan-(1→3)-α/βMan linkages (−36°). Similarly, the mean position of ψ in the two types of linkages differs by ∼10°, being on average +19° in the αMan-(1→2)-αMan linkages and +9° in the αMan-(1→3)-α/βMan linkages. The distributions of ϕ and ψ in αMan-(1→3)-α/βMan linkages, reflected in the CSDs, are slightly larger than those in αMan-(1→2)-αMan linkages, indicating greater flexibility in the α-(1→3) linkage. The mean positions of ϕ in all structures are consistent with expectations based on stereoelectronic considerations (the *exo*-anomeric effect[63−67] favors ϕ values near −60° in α-glycosides).

Parameterized *J*-coupling equations obtained from DFT calculations on **2**[c], and experimental *J*-couplings in **5**−**7**, were used to generate single-state models of ϕ and ψ in the αMan-(1→2)-αMan linkages in **5**−**7** (Figure 10). Essentially identical models were obtained for ϕ (∼−31° ± 12°) and ψ (19° ± 9°) for the αMan-(1→2)-αMan linkages in **2** and **5**−**7** (Table 3), indicating that terminal αMan-(1→2)-αMan linkages in oligosaccharides **5**−**7** assume conformations that are virtually identical to that found in reference disaccharide **2**.

Parameterized *J*-coupling equations obtained from DFT calculations on disaccharides **3**[c] and **4**[c], and experimental *J*-couplings (Table 2) in trisaccharides **6** and **8**, were used to

DOI: 10.1021/acs.biochem.8b01050
Biochemistry 2019, 58, 546−560

Table 3. Single-State von Mises Model Parameters (Mean Values and CSDs) and RMS Errors for *O*-Glycosidic Torsion Angles ϕ and ψ in 2−8 Determined From *MA'AT* Analyses of NMR *J*-Coupling Ensembles

	phi (ϕ)			psi (ψ)		
compd	mean ± SE (deg)[a]	CSD ± SE (deg)[b]	RMSD (Hz)[c]	mean ± SE (deg)	CSD ± SE (deg)	RMSD (Hz)
			αMan-(1→2)-αMan linkage			
2	−29.4 (±10.4)	25.2 (±13.3)	0.32	20.2 (±8.5)	22.0 (±10.0)	0.13
5	−29.6 (±12.0)	29.5 (±13.3)	0.30	16.9 (±9.1)	23.7 (±9.4)	0.30
6	−32.3 (±11.6)	28.8 (±13.7)	0.28	18.7 (±9.1)	23.9 (±9.5)	0.28
7	−32.0 (±11.8)	29.1 (±13.7)	0.24	19.5 (±8.9)	23.5 (±9.7)	0.24
average	**−31 (±12)**	**28 (±14)**	**0.29 (±0.03)**	**19 (±9)**	**23 (±10)**	**0.24 (±0.07)**
			αMan-(1→3)-α/βMan linkage			
3	−36.3 (±15.5)	35.8 (±13.5)	0.30	8.4 (±11.0)	26.9 (±9.4)	0.31
4	−36.5 (±13.9)	33.6 (±13.0)	0.25	10.2 (±10.6)	25.9 (±9.6)	0.28
6	−35.9 (±13.8)	33.4 (±15.5)	0.36	8.9 (±11.3)	27.9 (±9.4)	0.33
8	−36.4 (±12.3)	30.7 (±12.7)	0.31	9.7 (±10.7)	26.5 (±9.5)	0.28
average	**−36 (±14)**	**33 (±14)**	**0.31 (±0.04)**	**9 (±11)**	**27 (±10)**	**0.30 (±0.02)**

[a]SE = standard errors. [b]CSD = circular standard deviation. [c]RMSD = root mean squared deviation.

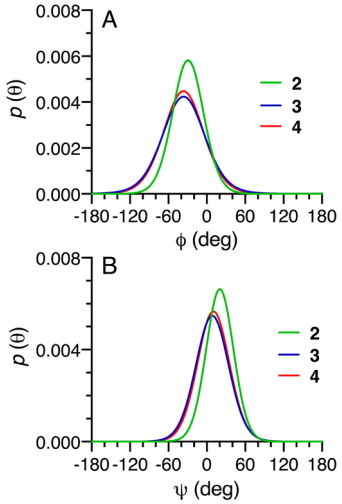

Figure 9. Single-state von Mises models of ϕ (A) and ψ (B) in disaccharides **2**−**4** determined from *MA'AT* analysis of trans-glycoside *J*-coupling ensembles.

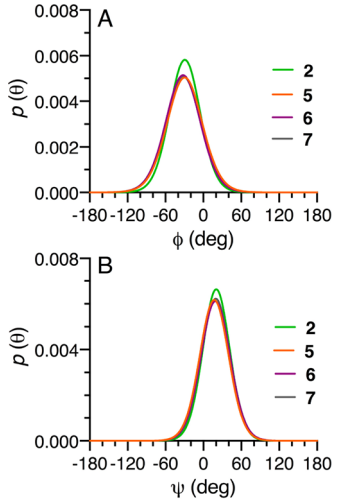

Figure 10. Single-state von Mises models of ϕ (A) and ψ (B) in the αMan-(1→2)-αMan linkages of disaccharide **2**, trisaccharides **5**−**6**, and tetrasaccharide **7** based on analyses of *J*-coupling ensembles.

Scheme 7. Mean Values of ϕ and ψ in αMan-(1→2)-αMan and αMan-(1→3)-α/βMan Linkages Obtained from *MA'AT* Analysis of Trans-glycosidic *J*-Couplings

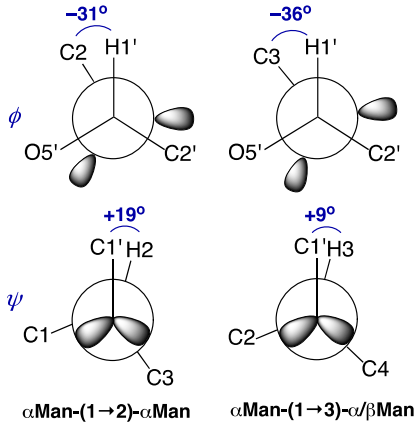

model ϕ and ψ in their constituent αMan-(1→3)-α/βMan linkages (Figure 11 and Table 3). The models for **3** and **4** are essentially identical to those for **6** and **8**. Thus, α-

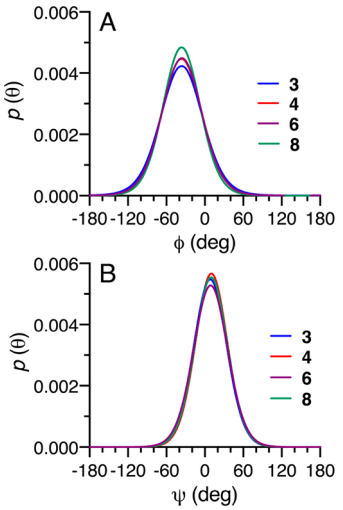

Figure 11. Single-state von Mises models of ϕ (A) and ψ (B) in the αMan-(1→3)-α/βMan linkages of disaccharides **3** and **4**, and trisaccharides **6** and **8**, based on analyses of *J*-coupling ensembles.

DOI: 10.1021/acs.biochem.8b01050
Biochemistry 2019, 58, 546−560

mannosylation at O2 of the αMan residue of **3** exerts virtually no effect on the conformation of the α-(1→3) linkage. Likewise α-mannosylation at O6 of the βMan residue of **4**, giving a 3,6-branched structure, exerts little effect on the conformation of the α-(1→3) linkage. While the context effects were found to be minor for both α-(1→2) and α-(1→3) linkages in the above comparisons, it is important to bear in mind that the extensions were modest in length and that larger, more complex extensions, which would provide greater opportunities for intramolecular interactions through structural folding (Scheme 2), are likely to elicit greater context effects.

In this work, single-state von Mises models were used to treat ϕ and ψ. Two parameters, the mean value and CSD, are obtained from this treatment, which allows a determination of the uniqueness of the model by visual inspection of the parameter space (Figures S11 and S12, Supporting Information). Unique solutions were observed for ϕ in all compounds. On the other hand, the parameter space of ψ typically contained two or three minima, with the global minimum giving the smallest RMS error in all cases. The existence of local minima complicates determinations of the uniqueness of the solution, and results from the limited number of experimental observables (in this case, three *J*-couplings) used to derive the model. Additional structure constraints such as nuclear Overhauser effects (NOEs) and/or residual dipolar couplings (RDCs) might help to reduce and/or eliminate these local minima. Additional *J*-coupling constraints may also improve the modeling; for example, for the αMan-(1→3)-α/βMan linkage, $^{2}J_{H1',C2'}$ may serve as an additional constraint on ϕ, while $^{2}J_{C2,H3}$, $^{2}J_{C4,H3}$, and $^{2}J_{C2,C4}$ may serve as constraints on ψ (Scheme 6).[18,71]

Behavior of ϕ and ψ in Disaccharides 2−4 and Tetrasaccharide 7 Determined from Aqueous MD Simulations and Crystal Structure Database Analysis. The behaviors of ϕ and ψ predicted from aqueous 1-μs MD simulations on **2**−**4** and **7** are shown in Figure 12 and summarized in Table S11 (Supporting Information). Mean values of ϕ in **2**−**4** and **7** obtained from MD trajectories are uniformly more negative by 9−15° than the NMR-determined means (Table 3), and CSDs determined from MD trajectories are smaller by 13−21° than those obtained from *MA'AT* analysis (Table 3). These findings suggest that the GLYCAM06 force field used to obtain the MD data may need adjustment to bring the calculated means of ϕ and the librational motion about these means into better alignment with experimental data. The NMR data indicate greater motional averaging about ϕ in both αMan-(1→2)-αMan and αMan-(1→3)-α/βMan *O*-glycosidic linkages than predicted by MD simulation. Similar observations were made recently in similar comparisons of NMR- and MD-determined behaviors of ϕ in β-(1→4) linkages.[15,71]

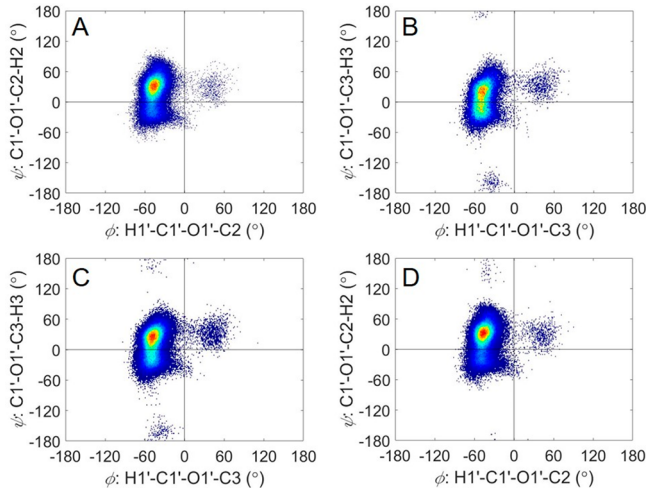

Figure 12. Distributions of ϕ and ψ obtained from aqueous MD simulations of disaccharides **2** (A), **3** (B), and **4** (C) and of the αMan-(1→2)-αMan linkage in **7** (D). Mean positions of ϕ are −44.6°, −45.7°, −46.9°, and −44.9° for **2**, **3**, **4**, and **7**, respectively. Mean positions of ψ are 20.9°, 7.2°, 10.1°, and 21.7° for **2**, **3**, **4**, and **7**, respectively (see Table S11, Supporting Information).

In contrast to ϕ, mean values of ψ obtained by MD simulation compare favorably with values determined from *MA'AT* analysis (Table S11; Supporting Information). For example, mean values of ψ for the αMan-(1→2)-αMan linkages in **2** and **7** were found by MD to be 21° and 22°, respectively, compared to 20.2° and 19.5°, respectively, by NMR *J*-coupling analysis. Likewise, for αMan-(1→3)-α/βMan linkages, mean values of ψ in **3** and **4** were found to be 7° and 10° by MD simulation, respectively, compared to 8° and 10°, respectively, by *MA'AT* analysis. In addition, CSD values for ψ determined by MD and NMR in **2**−**4** and **7** are in good agreement, especially for **3**, **4** and **7** (Table S11, Supporting Information). Collectively, these results illustrate the power of *MA'AT* analysis in allowing direct comparison of mean values and librational motions of *O*-glycosidic torsion angles in oligosaccharides to equivalent parameters derived from MD simulation, thus providing an experimental tool to validate the MD predictions.

A closer inspection of the MD histograms for **2**−**4** and **7** reveals Gaussian-like single-state distributions of the ϕ torsion angles that are qualitatively consistent with the NMR models, but the ψ distributions are bimodal (two overlapping Gaussian distributions) (Figure 13). This bimodal behavior is observed for both the αMan-(1→2)-αMan and the αMan-(1→3)-α/βMan linkages. The single-state von Mises distributions determined from *MA'AT* analyses overlap the MD-derived bimodal distributions very well but do not capture the fine structure predicted by MD. In the present work, it is not possible to determine whether the bimodal distributions of ψ are accurate representations of solution behavior because the number of experimental constraints used to model ψ is too small to test multistate models. The RMSDs for the *MA'AT* models are slightly lower than the RMSDs back-calculated from the MD simulations (Tables S7−S9, Supporting Information), but the differences are insignificant for all but one model. Additional experimental constraints in the form of *J*-couplings, nuclear Overhauser effects (NOEs),[43,44] residual dipolar couplings (RDCs),[12,45,46] and/or residual chemical shift anisotropy (RCSAs)[45,47−49] may allow multistate models to be tested in the future.

An analysis of ∼1700 oligosaccharide crystal structures containing αMan-(1→2)-αMan or αMan-(1→3)-α/βMan *O*-glycosidic linkages was conducted to obtain statistical distributions of ϕ and ψ in the solid state for comparison to those obtained by *MA'AT* analysis and MD simulation. Table S12 (Supporting Information) and Figure 14. The mean values of ϕ are in slightly better agreement with those obtained from MD simulation, whereas the CSDs are in better agreement with those obtained from *MA'AT* analysis. The mean values of ψ are in good agreement with those determined by both

DOI: 10.1021/acs.biochem.8b01050
Biochemistry 2019, 58, 546−560

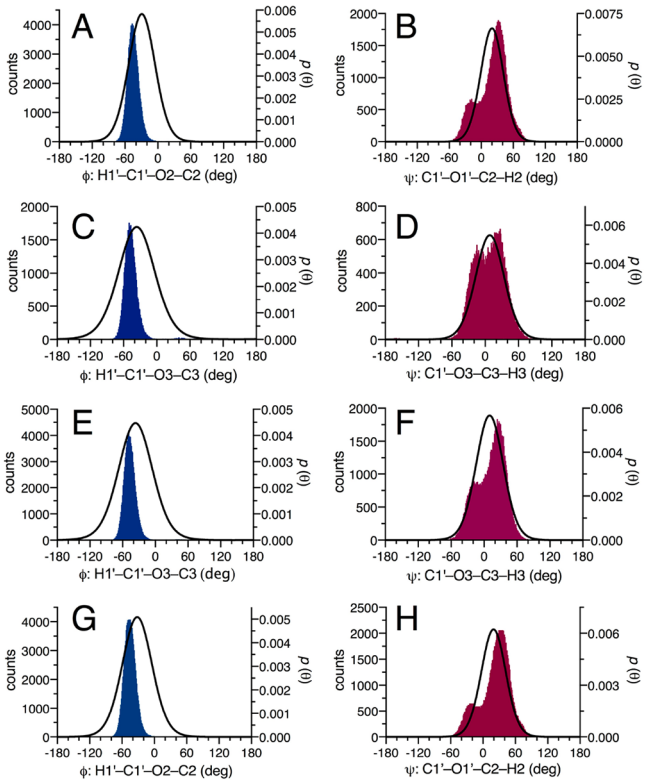

Figure 13. Distributions of ϕ and ψ obtained from aqueous 1 μs MD simulations (solid curves) superimposed on the same distributions obtained from *MA'AT* analysis (blue lines) for **2** (A and B), **3** (C and D), **4** (E and F), and the αMan-(1→2)-αMan linkage in **7** (G and H). See Tables 3 and and S11 (Supporting Information) for the mean values and CSDs for ϕ and ψ determined by NMR and MD in each compound.

MA'AT analysis and MD simulation, with values for αMan-(1→2)-αMan linkages being ∼10° larger than values for αMan-(1→3)-α/βMan linkages. CSD values for ψ determined from crystal structure analysis are slightly larger, on average, than those obtained by *MA'AT* analysis and MD simulation.

CONCLUSIONS

N-Glycan **1** contains 10 *O*-glycosidic linkages, four of which are αMan-(1→2)-αMan linkages and two of which are αMan-(1→3)-α/βMan linkages. The impact of these two linkage types on the overall conformational properties of **1** is therefore high, thus explaining the attention devoted to their conformations over the past 30 years.[72−90] Multiple experimental and computational methods have been brought to bear on the problem, leading to a range of models for compounds free in solution, in the crystalline state, or bound to protein receptors. The latter receptors have been typically ConA and cyanovirin, both of which bind αMan oligomers containing α-(1→2) glycosidic linkages. These data are summarized in Table S6 in the Supporting Information. For α-(1→2) linkages, the behavior of phi is fairly uniform; the averages of values in Table S6 are −29° ± 33° and −33° ± 16° for free and bound states, with ranges of −60° to 40° and −4° ± 50°, respectively. Thus, in general, phi favors values in the −60° regime (as expected based on stereoelectronic considerations), with occasional values in the +60° regime. The reported behavior of psi is also highly variable. Average values are 12° ± 36° and 23° ± 23° for free and bound states, with ranges of

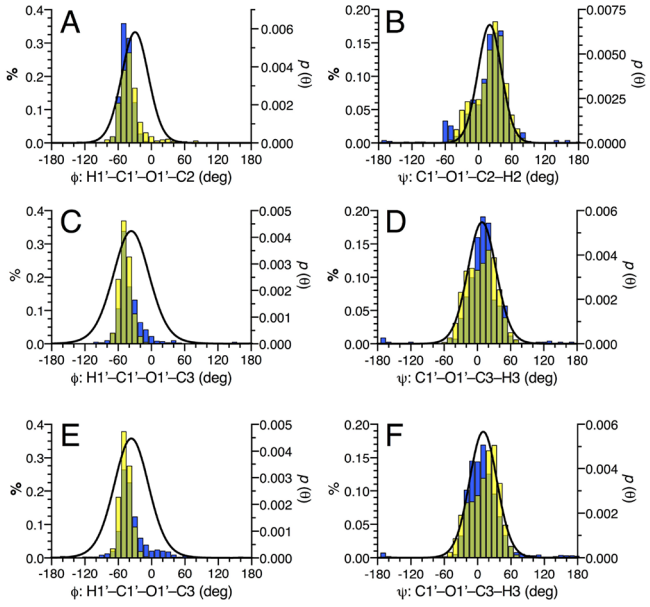

Figure 14. Overlays of MD (blue), crystal structure (yellow), and *MA'AT* (black line) distributions of the ϕ and ψ values for the *O*-glycosidic linkages in αMan-(1→2)-αManOCH$_3$ (**2**) (A and B), αMan-(1→3)-αManOCH$_3$ (**3**) (C and D), and αMan-(1→3)-βManOCH$_3$ (**4**) (E and F). The results for ψ show good agreement between the three data sets, but the *MA'AT* distribution for ϕ is significantly broader than those predicted by MD and from crystal structure database analyses.

−60° to 60° and −27° to 46°, respectively. In general, the +60° regime is more common than the −60° regime, but even recent NMR studies of **2** report up to 25% of the solution conformers having a psi torsion of ∼−30°.[87] Indeed, protein-bound αMan-(1→2)-αMan linkages appear to adopt negative psi values in some cases, and aqueous solutions of ligand containing a mix of 60°/−60° psi states might arguably promote receptor binding by providing both states in reasonable abundance at equilibrium. X-ray studies of **2** revealed a −54°/15° conformer, while a statistical analysis of the crystallographic database gave a −48°/16° favored conformation but also a fairly highly populated −58°/−55° conformer. Thus, while nearly 20 studies of the αMan-(1→2)-αMan linkage have been reported, significant uncertainties remain about the solution behavior of this linkage.

In contrast to αMan-(1→2)-αMan linkages, limited work has been reported on αMan-(1→3)-α/βMan linkages (Table S6). If the 1987 study[72] by the Homans group is ignored due to uncertainties about definitions, phi appears to favor values in the −60° regime, but psi appears to adopt values in both the +60° and −60° regimes. For example, in the α-anomer of **8**, two conformational states for the αMan-(1→3)-αMan linkage have been proposed that are equally populated: −60°/−60° and −40°/20°.[90] The only available crystal structure of a αMan-(1→3)-α/βMan disaccharide is one recently obtained in this laboratory on αMan-(1→3)-2-*O*-acetyl-βManOCH$_3$ monohydrate (**9**), which was monoacetylated to promote crystallization; linkage conformation in **9** is −43°/−6°.

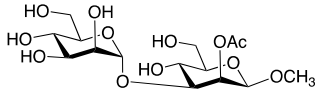

α-Man-(1→3)-2-*O*-acetyl-β-ManOCH$_3$ (**9**)

DOI: 10.1021/acs.biochem.8b01050
Biochemistry 2019, 58, 546−560

In this work, a new experimental method has been applied to investigate the behaviors of αMan-(1→2)-αMan and αMan-(1→3)-α/βMan *O*-glycosidic linkages in disaccharides **2**−**4** in which context effects are considered to be zero, and in somewhat larger oligomers (**5**−**8**) containing these linkages in which context effects may occur. Statistical analysis of the current X-ray databases was also performed, as well as 1 μs aqueous MD simulations of the three disaccharides and tetrasaccharide **7**. These results are superimposed in Figure 14. Free in solution, the *MA'AT* analyses indicate that all of the linkages studied highly favor a single conformational state, but libration about each of the mean values is significant. Mean and CSD values for ψ determined by all three techniques are in close agreement, although it appears that *MA'AT* analysis yields a slightly more librationally constrained ψ in **2** compared to MD and x-ray, as indicated by the smaller CSD value. Several x-ray structures that contain αMan-(1→2)-αMan linkages revealed −60°-regime conformers of ψ that were not detected by *MA'AT* or MD. Mean values of ϕ are slightly more positive than suggested by MD and X-ray, and the degree of libration determined from *MA'AT* analysis is considerably greater than indicated from MD and X-ray data. These findings are in close agreement with those found for β-(1→4) linkages.[15] Collectively these results indicate that, at least for αMan-(1→2)-αMan, αMan-(1→3)-α/βMan and approximately 15 β-(1→4) linkages examined to date using *MA'AT* analysis, some attention may need to be paid to adjusting the GLYCAM06 force field to bring the MD results in better alignment with the *MA'AT* models. The extent to which force fields other than GLYCAM06 compare with *MA'AT*-derived conformational models of ϕ and ψ in Man-containing oligosaccharides remains to be determined. Other experimental methods that are capable of yielding explicit conformational models of ϕ or ψ in *O*-glycosidic linkages are not available, so comparing *MA'AT*-derived models to other experiment-based models is not yet possible. However, as the method is further refined with the inclusion of additional experimental constraints such as RDCs and RCSAs, the resulting improved models will allow more rigorous testing of the structural conclusions drawn in this study.

It is noteworthy that linkage conformations in crystalline **2** (−54°/15°)[73] and crystalline **9** (−43°/−6°) (Table S6) are similar to those found in aqueous solution for **2**−**4**, although mean values for either ϕ or ψ are shifted by as much as ∼20°. This observation indicates that crystal packing effects perturb structure relative to that found in aqueous solution, presumably due to multiple and persistent H-bonding interactions in the crystal that differ in number and strength from the transient H-bonding interactions that occur in aqueous solution.

The number of *J*-couplings used in this work to determine the behaviors of ϕ and ψ in di- and oligosaccharides supported the use of single-state but not multistate models in *MA'AT* analysis. A legitimate concern might be whether two- or three-state models pertain in some cases. While multistate models cannot be excluded, the RMSDs obtained from single-state models were small (≤0.4 Hz), which shows that these models fit the available data well. Employing multistate models to treat ϕ and ψ will require more experimental observables, perhaps in the form of additional *J*-couplings and/or other NMR parameters such as chemical shifts, residual dipolar couplings, NOEs and/or residual chemical shift anisotropies. It is expected that incorporation of the latter NMR parameters as additional constraints in *MA'AT* analysis will allow multistate models of glycosidic torsion angles to be investigated.

A question that might arise is whether *MA'AT* analysis is sufficiently sensitive to detect a second, minor linkage conformer in aqueous solutions of **2**, as suggested in recent studies by Säwén et al.[87] In this prior work, the dominant conformer (−40°/33°; 75%), which is similar to that determined in this work (−29°/20°; Table 3), was reported to coexist with a minor conformer (−40°/∼ −30°; ∼25%). The RMSD values for this two-state model were back-calculated using parameterized *J*-coupling equations and average CSDs typically obtained from *MA'AT* analyses. The calculated RMSDs for ϕ and ψ (0.53 and 0.52 Hz, respectively) were significantly larger than those obtained from *MA'AT*-derived single-state models, indicating that the fractional population of minor conformers in solution is probably less than 25%.

One advantage of redundant *J*-couplings as linkage conformational probes is that visual inspections of ensembles sensitive to either ϕ or ψ allow rapid qualitative assessments of the extent to which a given linkage in different structural contexts changes in conformation. In the present work, we found that context effects within the relatively limited set of oligosaccharides **5**−**8** were small, and this conclusion was supported by subsequent quantitative studies using the *MA'AT* algorithm. As oligosaccharides increase in size and complexity, it will be interesting to determine to what extent the linkages are perturbed from the reference (disaccharide) states, and equally important, to what extent librational motions are either enhanced or suppressed. Since intermolecular interactions with solvent, and intramolecular interactions (e.g., H-bonding) are likely to increase in importance with increasing molecular weight and complexity, and since their numbers and strengths will depend on structure, it is difficult to predict how these context effects will be expressed. Nevertheless, this work describes a promising new experimental tool to investigate these effects in molecules such as **1** for which current knowledge of conformational equilibria and dynamics based on experimental measurements remain rudimentary but whose conformational properties are expected to be tightly coupled to their biological functions.

■ ASSOCIATED CONTENT

Supporting Information

The Supporting Information is available free of charge on the ACS Publications website at DOI: 10.1021/acs.biochem.8b01050.

Synthetic procedures to prepare $\mathbf{2}^{1',2'}$, $\mathbf{3}^{3,1'}$, $\mathbf{4}^{1'}$, $\mathbf{4}^{2'}$, $\mathbf{5}^{2',1''}$, $\mathbf{6}^{2',1''}$, $\mathbf{6}^{3,1'}$, $\mathbf{7}^{2'',1'''}$, $\mathbf{8}^{1'}$, and $\mathbf{8}^{2'}$; NMR spectra of $\mathbf{5}^{2',1''}$, $\mathbf{6}^{2',1''}$, $\mathbf{3}^{1',3}$, $\mathbf{6}^{3,1'}$, and $\mathbf{6}^{3,1'}$; ^{1}H and ^{13}C chemical shifts in **2**−**4**; ^{1}H−^{1}H spin-coupling constants in **2**−**4**; ^{13}C−^{1}H and ^{13}C−^{13}C spin-coupling constants in **2**−**4**; torsional constraints applied to $\mathbf{2}^{c}$−$\mathbf{4}^{c}$ during DFT calculations; hypersurfaces for ϕ-dependent *J*-couplings in $\mathbf{2}^{c}$−$\mathbf{4}^{c}$; hypersurfaces for ψ-dependent *J*-couplings in $\mathbf{2}^{c}$−$\mathbf{4}^{c}$; parameter space for single-state models of ϕ and ψ in αMan-(1→2)-αMan and αMan-(1→3)-α/βMan linkages; aqueous MD simulation histograms for ϕ and ψ in **2**−**4** and **7**; tables of back-calculated *J*-couplings from MD simulations; ^{1}H and ^{13}C chemical shifts in **5**−**8**; behavior of ϕ and ψ in **2**−**4** and **7** from MD simulations;

DOI: 10.1021/acs.biochem.8b01050
Biochemistry 2019, 58, 546−560

statistical analysis of ϕ and ψ crystal structures containing Man-Man linkages; measurement of *trans*-glycosidic J_{CH} and J_{CC}; Cartesian coordinates for DFT-optimized conformers of $\mathbf{2}^{c}-\mathbf{4}^{c}$ (PDF)

AUTHOR INFORMATION

Corresponding Author

*E-mail: aseriann@nd.edu.

ORCID

Robert J. Woods: 0000-0002-2400-6293

Anthony S. Serianni: 0000-0001-6114-1446

Funding

Financial support was provided by the National Science Foundation (CHE 1402744 and 1707660 to A.S.) and by Omicron Biochemicals, Inc.

Notes

The authors declare no competing financial interest.

ACKNOWLEDGMENTS

The Notre Dame Radiation Laboratory is supported by the Department of Energy Office of Science, Office of Basic Energy Sciences under Award Number DE-FC02-04ER15533. This is document number NDRL 5221.

REFERENCES

(1) Nagae, M., and Yamaguchi, Y. (2012) Function and 3D Structure of the *N*-Glycans on Glycoproteins. *Int. J. Mol. Sci. 13*, 8398−8429.

(2) Clerc, F., Reiding, K. R., Jansen, B. C., Kammeijer, G. S. M., Bondt, A., and Wuhrer, M. (2016) Human Plasma Protein *N*-Glycosylation. *Glycoconjugate J. 33*, 309−343.

(3) Satoh, T., Yamaguchi, T., and Kato, K. (2015) Emerging Structural Insights into Glycoprotein Quality Control Coupled with *N*-Glycan Processing in the Endoplasmic Reticulum. *Molecules 20*, 2475−2491.

(4) Bolmstedt, A. J., O'Keefe, B. R., Shenoy, S. R., McMahon, J. B., and Boyd, M. R. (2001) Cyanovirin-N Defines a New Class of Antiviral Agent Targeting *N*-Linked, High-Mannose Glycans in an Oligosaccharide-Specific Manner. *Mol. Pharmacol. 59*, 949−954.

(5) Jitsuhara, Y., Toyoda, T., Itai, T., and Yamaguchi, H. (2002) Chaperone-Like Functions of High-Mannose Type and Complex-Type *N*-Glycans and Their Molecular Basis. *J. Biochem. 132*, 803−811.

(6) Wyss, D. F., Choi, J. S., Li, J., Knoppers, M. H., Willis, K. J., Arulanandam, A. R., Smolyar, A., Reinherz, E. L., and Wagner, G. (1995) Conformation and Function of the *N*-Linked Glycan in the Adhesion Domain of Human CD2. *Science 269*, 1273−1278.

(7) Hanson, S. R., Culyba, E. K., Hsu, T.-L., Wong, C.-H., Kelly, J. W., and Powers, E. T. (2009) The Core Trisaccharide of an *N*-Linked Glycoprotein Intrinsically Accelerates Folding and Enhances Stability. *Proc. Natl. Acad. Sci. U. S. A. 106*, 3131−3136.

(8) Recny, M. A., Luther, M. A., Knoppers, M. H., Neidhardt, E. A., Khandekar, S. S., Concino, M. F., Schimke, P. A., Francis, M. A., Moebius, U., Reinhold, B. B., Reinhold, V. N., and Reinherz, E. L. (1992) *N*-Glycosylation Is Required for Human CD2 Immunoadhesion Functions. *J. Biol. Chem. 267*, 22428−22434.

(9) Sakae, Y., Satoh, T., Yagi, H., Yanaka, S., Yamaguchi, T., Isoda, Y., Iida, S., Okamoto, Y., and Kato, K. (2017) Conformational Effects of *N*-Glycan Core Fucosylation of Immunoglogulin G Fc Region on Its Interaction with Fcγ Receptor IIIa. *Sci. Rep. 7*, 13780.

(10) Wormald, M. R., Petrescu, A. J., Pao, Y.-L., Glithero, A., Elliott, T., and Dwek, R. A. (2002) Conformational Studies of Oligosaccharides and Glycopeptides: Complementarity of NMR, X-ray Crystallography, and Molecular Modeling. *Chem. Rev. 102*, 371−386.

(11) Frank, M., Collins, P. M., Peak, I. R., Grice, I. D., and Wilson, J. C. (2015) An Unusual Carbohydrate Conformation Is Evident in *Moraxella catarrhalis* Oligosaccharides. *Molecules 20*, 14234−14253.

(12) Tian, F., Al-Hashimi, H. M., Craighead, J. L., and Prestegard, J. H. (2001) Conformational Analysis of a Flexible Oligosaccharide Using Residual Dipolar Couplings. *J. Am. Chem. Soc. 123*, 485−492.

(13) Bose, B., Zhao, S., Stenutz, R., Cloran, F., Bondo, P. B., Bondo, G., Hertz, B., Carmichael, I., and Serianni, A. S. (1998) Three-Bond C−O−C−C Spin-Coupling Constants in Carbohydrates: Development of a Karplus Relationship. *J. Am. Chem. Soc. 120*, 11158−11173.

(14) Cloran, F., Carmichael, I., and Serianni, A. S. (1999) Density Functional Calculations on Disaccharide Mimics: Studies of Molecular Geometries and Trans-*O*-Glycosidic $^{3}J_{COCH}$ and $^{3}J_{COCC}$ Spin-Couplings. *J. Am. Chem. Soc. 121*, 9843−9851.

(15) Zhang, W., Turney, T., Meredith, R., Pan, Q., Sernau, L., Wang, X., Hu, X., Woods, R. J., Carmichael, I., and Serianni, A. S. (2017) Conformational Populations of β-(1→4) *O*-Glycosidic Linkages Using Redundant NMR *J*-Couplings and Circular Statistics. *J. Phys. Chem. B B121*, 3042−3058.

(16) Jardetzky, O. (1980) On the Nature of Molecular Conformations Inferred from High-Resolution NMR. *Biochim. Biophys. Acta, Protein Struct. 621*, 227−232.

(17) Bürgi, R., Pitera, J., and van Gunsteren, W. F. (2001) Assessing the Effect of Conformational Averaging on the Measured Values of Observables. *J. Biomol. NMR 19*, 305−320.

(18) Hadad, M. J., Zhang, W., Turney, T., Sernau, L., Wang, X., Woods, R. J., Incandela, A., Surjancev, I., Wang, A., Yoon, M.-K., Coscia, A., Euell, C., Meredith, R., Carmichael, I., and Serianni, A. S. (2017) NMR Spin-Couplings in Saccharides: Relationships Between Structure, Conformation and the Magnitudes of J_{HH}, J_{CH} and J_{CC} Values. In *New Developments in NMR 10: NMR in Glycoscience and Glycotechnology* (Peters, T., and Kato, K., Eds.), pp 20−100, Royal Society of Chemistry.

(19) Klepach, T., Zhao, H., Hu, X., Zhang, W., Stenutz, R., Hadad, M. J., Carmichael, I., and Serianni, A. S. (2015) Informing Saccharide Structural NMR Studies with Density Functional Theory Calculations. In *Glycoinformatics: Methods in Molecular Biology* (Lütteke, T., and Frank, M. Eds.), pp 289−331, Springer, New York.

(20) Karplus, M. (1959) Contact Electron-Spin Coupling of Nuclear Magnetic Moments. *J. Chem. Phys. 30*, 11−15.

(21) Turney, T., Pan, Q., Sernau, L., Carmichael, I., Zhang, W., Wang, X., Woods, R. J., and Serianni, A. S. (2017) *O*-Acetyl Side-Chains in Monosaccharides: Redundant NMR Spin-Couplings and Statistical Models for Acetate Ester Conformational Analysis. *J. Phys. Chem. B B121*, 66−77.

(22) Serianni, A. S., Nunez, H. A., and Barker, R. (1979) Carbon-13-Enriched Carbohydrates. Preparation of Aldononitriles and Their Reduction with a Palladium Catalyst. *Carbohydr. Res. 72*, 71−78.

(23) Hayes, M. L., Pennings, N. A., Serianni, A. S., and Barker, R. (1982) Epimerization of Aldoses by Molybdate Involving a Novel Rearrangement of the Carbon Skeleton. *J. Am. Chem. Soc. 104*, 6764−6769.

(24) Zhang, W., Zhao, S., and Serianni, A. S. (2015) Labeling Monosaccharides With Stable Isotopes. *Methods Enzymol. 565*, 423−458.

(25) Zhang, W. (2009) Solution Studies of Monosaccharide and Oligosaccharide Structure and Reactivity by NMR Spectroscopy. Doctoral dissertation, retrieved from https://search.proquest.com/docview/849759226?pq-origsite=gscholar.

(26) Zhang, W., Pan, Q., and Serianni, A. S. (2016) A Chemical Synthesis of a Multiply ^{13}C-Labeled Hexasaccharide: A High-Mannose *N*-Glycan Fragment. *J. Labelled Compd. Radiopharm. 59*, 673−679.

(27) Bock, K., and Pedersen, C. (1977) Two- and Three-Bond ^{13}C−^{1}H Couplings in Some Carbohydrates. *Acta Chem. Scand. B31*, 354−358.

(28) Church, T., Carmichael, I., and Serianni, A. S. (1996) Two-Bond ^{13}C-^{13}C Spin-Coupling Constants in Carbohydrates: Effect of

DOI: 10.1021/acs.biochem.8b01050
Biochemistry 2019, 58, 546−560

Structure on Coupling Magnitude and Sign. *Carbohydr. Res. 280*, 177−186.
(29) Meissner, A., and Sørensen, O. W. (2001) Measurement of *J*(H,H) and Long-range *J*(X,H) Coupling Constants in Small Molecules. Broadband XLOC and J-HMBC. *Magn. Reson. Chem. 39*, 49−52.
(30) Frisch, M. J., Trucks, G. W., Schlegel, H. B., Scuseria, G. E., Robb, M. A., Cheeseman, J. R., Scalmani, G., Barone, V., Mennucci, B., Petersson, G. A., Nakatsuji, H., Caricato, M., Li, X., Hratchian, H. P., Izmaylov, A. F., Bloino, J., Zheng, G., Sonnenberg, J. L., Hada, M., Ehara, M., Toyota, K., Fukuda, R., Hasegawa, J., Ishida, M., Nakajima, T., Honda, Y., Kitao, O., Nakai, H., Vreven, T., Montgomery, J. A., Jr., Peralta, J. E., Ogliaro, F., Bearpark, M., Heyd, J. J., Brothers, E., Kudin, K. N., Staroverov, V. N., Kobayashi, R., Normand, J., Raghavachari, K., Rendell, A., Burant, J. C., Iyengar, S. S., Tomasi, J., Cossi, M., Rega, N., Millam, J. M., Klene, M., Knox, J. E., Cross, J. B., Bakken, V., Adamo, C., Jaramillo, J., Gomperts, R., Stratmann, R. E., Yazyev, O., Austin, A. J., Cammi, R., Pomelli, C., Ochterski, J. W., Martin, R. L., Morokuma, K., Zakrzewski, V. G., Voth, G. A., Salvador, P., Dannenberg, J. J., Dapprich, S., Daniels, A. D., Farkas, Ö., Foresman, J. B., Ortiz, J. V., Cioslowski, J., and Fox, D. J. (2009) *Gaussian09*, Revision E.01, Gaussian, Inc., Wallingford CT.
(31) Becke, A. D. (1993) Density-Functional Thermochemistry. III. The Role of Exact Exchange. *J. Chem. Phys. 98*, 5648−5652.
(32) Hehre, W. J., Ditchfield, R., and Pople, J. A. (1972) Self-Consistent Molecular Orbital Methods. XII. Further Extensions of Gaussian-Type Basis Sets for Use in Molecular Orbital Studies of Organic Molecules. *J. Chem. Phys. 56*, 2257−2261.
(33) Cances, E., Mennucci, B., and Tomasi, J. (1997) A New Integral Equation Formalism for the Polarizable Continuum Model: Theoretical Background and Applications to Isotropic and Anisotropic Dielectrics. *J. Chem. Phys. 107*, 3032−3041.
(34) Cammi, R., Mennucci, B., and Tomasi, J. (2000) Fast Evaluation of Geometries and Properties of Excited Molecules in Solution: A Tamm-Dancoff Model with Application to 4 Dimethylaminobenzonitrile. *J. Phys. Chem. A A104*, 5631−5637.
(35) Sychrovsky, V., Grafenstein, J., and Cremer, D. (2000) Nuclear Magnetic Resonance Spin−Spin Coupling Constants from Coupled Perturbed Density Functional Theory. *J. Chem. Phys. 113*, 3530−3547.
(36) Helgaker, T., Watson, M., and Handy, N. C. (2000) Analytical Calculation of Nuclear Magnetic Resonance Indirect Spin−Spin Coupling Constants at the Generalized Gradient Approximation and Hybrid Levels of Density-Functional Theory. *J. Chem. Phys. 113*, 9402−9409.
(37) Barone, V., Peralta, J. E., Contreras, R. H., and Snyder, J. P. (2002) DFT Calculation of NMR J_{FF} Spin−Spin Coupling Constants in Fluorinated Pyridines. *J. Phys. Chem. A A106*, 5607−5612.
(38) Stenutz, R., Carmichael, I., Widmalm, G., and Serianni, A. S. (2002) Hydroxymethyl Group Conformation in Saccharides: Structural Dependencies of $^{2}J_{HH}$, $^{3}J_{HH}$ and $^{1}J_{CH}$ Spin-Spin Coupling Constants. *J. Org. Chem. 67*, 949−958.
(39) *Prism 5 for Mac OS X*, GraphPad Software, Version 5.0d, November 8, 2010.
(40) Jones, E., Oliphant, T., and Peterson, P. (2014) *SciPy: Open Source Scientific Tools for Python*.
(41) Agostinelli, C., and Lund, U. (2011) *R Package Circular: Circular Statistics* (version 0.4-3). CA: Department of Environmental Sciences, Informatics and Statistics, Ca'Foscari University, Venice, Italy. UL: Department of Statistics, California Polytechnic State University: San Luis Obispo, California.
(42) Pewsey, A., Neuhäuser, M., and Ruxton, G. D. (2013) *Circular Statistics in R*, Oxford University Press.
(43) Yuen, K. (2010) *Bayesian Methods for Structural Dynamics and Civil Engineering*, pp 257−262, Wiley.
(44) Patel, D. S., Pendrill, R., Mallajosyula, S. S., Widmalm, G., and MacKerell, A. D., Jr. (2014) Conformational Properties of α-or β-(1→6)-Linked Oligosaccharides: Hamiltonian Replica Exchange MD Simulations and NMR Experiments. *J. Phys. Chem. B B118*, 2851−2871.
(45) Höög, C., Landersjö, C., and Widmalm, G. (2001) Oligosaccharides Display Both Rigidity and High Flexibility in Water as Determined by ^{13}C NMR Relaxation and ^{1}H,^{1}H NOE Spectroscopy: Evidence of anti-ϕ and anti-ψ Torsions in the Same Glycosidic Linkage. *Chem. - Eur. J. 7*, 3069−3077.
(46) Liu, Y., and Prestegard, J. H. (2010) A Device for the Measurement of Residual Chemical Shift Anisotropy and Residual Dipolar Coupling in Soluble and Membrane-Associated Proteins. *J. Biomol. NMR 47*, 249−258.
(47) Freedberg, D. I. (2002) An Alternative Method for Pucker Determination in Carbohydrates from Residual Dipolar Couplings: A Solution NMR Study of the Fructofuranosyl Ring of Sucrose. *J. Am. Chem. Soc. 124*, 2358−2362.
(48) Lipsitz, R. S., and Tjandra, N. (2001) Carbonyl CSA Restraints from Solution NMR for Protein Structure Refinement. *J. Am. Chem. Soc. 123*, 11065−11066.
(49) Lipsitz, R. S., and Tjandra, N. (2003) ^{15}N Chemical Shift Anisotropy in Protein Structure Refinement and Comparison with NH Residual Dipolar Couplings. *J. Magn. Reson. 164*, 171−176.
(50) Complex Carbohydrate Research Center (CCRC), University of Georgia, http://www.glycam.org (Date last accessed June 27, 2018).
(51) Kirschner, K. N., Yongye, A. B., Tschampel, S. M., González-Outeiriño, J., Daniels, C. R., Foley, B. L., and Woods, R. J. (2008) GLYCAM06: A Generalizable Biomolecular Force Field. Carbohydrates. *J. Comput. Chem. 29*, 622−655.
(52) Jorgensen, W. L., Chandrasekhar, J., Madura, J. D., Impey, R. W., and Klein, M. L. (1983) Comparison of Simple Potential Functions for Simulating Liquid Water. *J. Chem. Phys. 79*, 926−935.
(53) Case, D. A., Babin, V., Berryman, J. T., Betz, R. M., Cai, Q., Cerutti, D. S., Cheatham, T. E. I., Darden, T. A., Duke, R. E., Gohlke, H., Goetz, A. W., Gusarov, S., Homeyer, N., Janowski, P., Kaus, J., Kolossváry, I., Kovalenko, A., Lee, T. S., LeGrand, S., Luchko, T., Luo, R., Madej, B., Merz, K. M., Paesani, F., Roe, D. R., Roitberg, A., Sagui, C., Salomon-Ferrer, R., Seabra, G., Simmerling, C. L., Smith, W., Swails, J., Walker, R. C., Wang, J., Wolf, R. M., Wu, X., and Kollman, P. A. (2014) *AMBER 14*, University of California, San Francisco.
(54) Berendsen, H. J. C., Postma, J. P. M., van Gunsteren, W. F., DiNola, A., and Haak, J. R. (1984) Molecular Dynamics with Coupling to an External Bath. *J. Chem. Phys. 81*, 3684−3690.
(55) van Gunsteren, W. F., and Berendsen, H. J. C. (1977) Algorithms for Macromolecular Dynamics and Constraint Dynamics. *Mol. Phys. 34*, 1311−1327.
(56) Götz, A. W., Williamson, M. J., Xu, D., Poole, D., Le Grand, S., and Walker, R. C. (2012) Routine Microsecond Molecular Dynamics Simulations with AMBER on GPUs. 1. Generalized Born. *J. Chem. Theory Comput. 8*, 1542−1555.
(57) Kirschner, K. N., and Woods, R. J. (2001) Solvent Interactions Determine Carbohydrate Conformation. *Proc. Natl. Acad. Sci. U. S. A. 98*, 10541−10545.
(58) Zhao, H., Carmichael, I., and Serianni, A. S. (2008) Oligosaccharide Trans-Glycoside $^{3}J_{COCC}$ Karplus Curves Are Not Equivalent: Effect of Internal Electronegative Substituents. *J. Org. Chem. 73*, 3255−3257.
(59) Edward, J. T. (1955) Stability of Glycosides to Acid Hydrolysis. *Chem. Ind. (London)*, 1102−1104.
(60) Lemieux, R. U., Kullnig, R. K., Bernstein, H. J., and Schneider, W. G. (1958) Configurational Effects on the Proton Magnetic Resonance Spectra of Six-Membered Ring Compounds. *J. Am. Chem. Soc. 80*, 6098−6105.
(61) Lemieux, R. (1971) Effects of Unshared Pairs of Electrons and Their Solvation on Conformational Equilibria. *Pure Appl. Chem. 25*, 527−548.
(62) Praly, J.-P., and Lemieux, R. (1987) Influence of Solvent on the Magnitude of the Anomeric Effect. *Can. J. Chem. 65*, 213−223.
(63) Thøgersen, H., Lemieux, R. U., Bock, K., and Meyer, B. (1982) Further Justification for the *Exo* Anomeric Effect. Conformational

DOI: 10.1021/acs.biochem.8b01050
Biochemistry 2019, 58, 546−560

Analysis Based on Nuclear Magnetic Resonance Spectroscopy of Oligosaccharides. *Can. J. Chem. 60*, 44−57.
(64) Kirby, A. J. (1983) *The Anomeric Effect and Related Stereoelectronic Effects at Oxygen*, Springer Verlag, Berlin.
(65) Alabugin, I. V. (2016) *Stereoelectronic Effects. A Bridge Between Structure and Reactivity*, John Wiley & Sons, West Sussex, UK.
(66) Graczyk, P. P., and Mikolajczyk, M. (1994) *Topics in Stereochemistry* (Eliel, E. L., and Wilen, S. H., Eds.), Vol. *21*, Wiley and Sons, New York, pp 159−349.
(67) Juaristi, E., and Cuevas, G. (1995) *The Anomeric Effect*, CRC Press, Boca Raton, FL.
(68) Cloran, F., Carmichael, I., and Serianni, A. S. (2000) $^{2}J_{COC}$ Spin-Spin Coupling Constants Across Glycosidic Linkages Exhibit a Valence Bond Angle Dependence. *J. Am. Chem. Soc. 122*, 396−397.
(69) King-Morris, M. J., and Serianni, A. S. (1987) ^{13}C NMR Studies of [1-^{13}C]Aldoses: Empirical Rules Correlating Pyranose Ring Configuration and Conformation with ^{13}C Chemical Shifts and ^{13}C-^{13}C Couplings. *J. Am. Chem. Soc. 109*, 3501−3508.
(70) Wu, J., Bondo, P. B., Vuorinen, T., and Serianni, A. S. (1992) ^{13}C-^{13}C Spin Coupling Constants in Aldoses Enriched with ^{13}C at the Terminal Hydroxymethyl Carbon: Effect of Coupling Pathway Structure on J_{CC} in Carbohydrates. *J. Am. Chem. Soc. 114*, 3499−3505.
(71) Zhang, W., Meredith, R., Yoon, M.-K., Wang, X., Woods, R. J., Carmichael, I., and Serianni, A. S. (2019) Synthesis and *O*-Glycosidic Linkage Conformational Analysis of ^{13}C-Labeled Oligosaccharide Fragments of an Antifreeze Glycolipid. *J. Org. Chem.*, DOI: 10.1021/acs.joc.8b01411.
(72) Homans, S. W., Pastore, A., Dwek, R. A., and Rademacher, T. W. (1987) Structure and Dynamics of Oligomannose-Type Oligosaccharides. *Biochemistry 26*, 6649−6655.
(73) Srikrishnan, T., Chowdhary, M. S., and Matta, K. L. (1989) Crystal and Molecular Structure of Methyl *O*-α-D-Mannopyranosyl-(1→2)-α-D-mannopyranoside. *Carbohydr. Res. 186*, 167−175.
(74) Edge, C. J., Singh, U. C., Bazzo, R., Taylor, G. L., Dwek, R. A., and Rademacher, T. W. (1990) 500 ps Molecular Dynamics in Water of the Manα1→2Manα Glycosidic Linkage Present in Asn-Linked Oligomannose-Type Structures on Glycoproteins. *Biochemistry 29*, 1971−1974.
(75) Peters, T. (1991) Synthesis and Conformational Analysis of Methyl 2-*O*-(α-D-Mannopyranosyl)-α-D-mannopyranoside. *Liebigs Ann. Chem. 1991*, 135−141.
(76) Stevens, E. S. (1994) The Potential Energy Surface of Methyl 2-*O*-(α-D-Mannopyranosyl)-α-D-Mannopyranoside in Aqueous Solution: Conclusions Derived from Optical Rotation. *Biopolymers 34*, 1403−1407.
(77) Dowd, M. K., French, A. D., and Reilly, P. J. (1995) Molecular Mechanics Modeling of α-(1→2), α-(1→3)-, and α-(1→6)-Linked Mannosyl Disaccharides with MM3(92). *J. Carbohydr. Chem. 14*, 589−600.
(78) Woods, R. J., Pathiaseril, A., Wormald, M. R., Edge, C. J., and Dwek, R. A. (1998) The High Degree of Internal Flexibility Observed for an Oligomannose Oligosaccharide Does Not Alter the Overall Topology of the Molecule. *Eur. J. Biochem. 258*, 372−386.
(79) Moothoo, D. N., Canan, B., Field, R. A., and Naismith, J. H. (1999) Manα1−2 Man α-OMe−Concanavalin A Complex Reveals a Balance of Forces Involved in Carbohydrate Recognition. *Glycobiology 9*, 539−545.
(80) Petrescu, A. J., Petrescu, S. M., Dwek, R. A., and Wormald, M. R. (1999) A Statistical Analysis of *N*- and *O*-Glycan Linkage Conformations From Crystallographic Data. *Glycobiology 9*, 343−352.
(81) Bewley, C. A. (2001) Solution Structure of a Cyanovirin-N:Manα1−2Manα Complex: Structural Basis for High-Affinity Carbohydrate-Mediated Binding to gp120. *Structure 9*, 931−940.
(82) Almond, A., Bunkenborg, J., Franch, T., Gotfredsen, C. H., and Duus, J. Ø. (2001) Comparison of Aqueous Molecular Dynamics with NMR Relaxation and Residual Dipolar Couplings Favors Internal Motion in a Mannose Oligosaccharide. *J. Am. Chem. Soc. 123*, 4792−4802.
(83) Botos, I., O'Keefe, B. R., Shenoy, S. R., Cartner, L. K., Ratner, D. M., Seeberger, P. H., Boyd, M. R., and Wlodawer, A. (2002) Structures of the Complexes of a Potent Anti-HIV Protein Cyanovirin-N and High Mannose Oligosaccharides. *J. Biol. Chem. 277*, 34336−34342.
(84) Lycknert, K., Helander, A., Oscarson, S., Kenne, L., and Widmalm, G. (2004) A Conformational Study of α-D-Man*p*-(1→2)-α-D-Man*p*-(1→*O*)-L-Ser by NMR ^{1}H,^{1}H T-ROESY Experiments and Molecular-Dynamics Simulations. *Carbohydr. Res. 339*, 1331−1338.
(85) Margulis, C. J. (2005) Computational Study of the Dynamics of Mannose Disaccharides Free in Solution and Bound to the Potent Anti-HIV Virucidal Protein Cyanovirin. *J. Phys. Chem. B B109*, 3639−3647.
(86) Fromme, R., Katiliene, Z., Giomarelli, B., Bogani, F., Mc Mahon, J., Mori, T., Fromme, P., and Ghirlanda, G. (2007) A Monovalent Mutant of Cyanovirin-N Provides Insight into the Role of Multiple Interactions with gp120 for Antiviral Activity. *Biochemistry 46*, 9199−9207.
(87) Säwén, E., Massad, T., Landersjö, C., Damberg, P., and Widmalm, G. (2010) Population Distribution of Flexible Molecules from Maximum Entropy Analysis Using Different Priors as Background Information: Application to the *ϕ*,*ψ*-Conformational Space of the α-(1→2)-Linked Mannose Disaccharide Present in *N*- and *O*-Linked Glycoproteins. *Org. Biomol. Chem. 8*, 3684−3695.
(88) Nestor, G., Anderson, T., Oscarson, S., and Gronenborn, A. M. (2017) Exploiting Uniformly ^{13}C-Labeled Carbohydrates For Probing Carbohydrate-Protein Interactions by NMR Spectroscopy. *J. Am. Chem. Soc. 139*, 6210−6216.
(89) Nestor, G., Anderson, T., Oscarson, S., and Gronenborn, A. M. (2018) Direct Observation of Carbohydrate Hydroxyl Proteins in Hydrogen Bonds With a Protein. *J. Am. Chem. Soc. 140*, 339−345.
(90) Sayers, E. W., and Prestegard, J. H. (2000) Solution Conformations of a Trimannoside From Nuclear Magnetic Resonance and Molecular Dynamics Simulations. *Biophys. J. 79*, 3313−3329.

DOI: 10.1021/acs.biochem.8b01050
Biochemistry 2019, 58, 546−560